Models for dark matter and Neutrino masses

Guillermo Palacio
Universidad de Antioquia

A dissertation submitted to the Universidad de Antioquia
for the degree of Doctor of Philosophy

Declaration

I declare that this thesis has been the result of my research done at Universidad de Antioquia and this thesis content has not be submitted for any other degree or professional qualification. The work submitted is my own, except where work which has formed part of jointly-authored publications has been included.

Guillermo Palacio

Acknowledgements

The realization of this thesis was possible first of all, to the collaboration of my advisor, Diego Restrepo, and asesors, Federico von der Pahlen and Oscar Zapata; who guided me through my PhD program time at Universidad de Antioquia. Their enthusiasm made the research effort not only challenging but also enjoyable. They motivated me to go beyond goals I had set for myself.

I thank to my family for their unconditional support and the lot of patient during this time. They motive me and inspired me to overcome all the difficulties on the way of life. This work would be impossible without the generous help of my colleague at Universidad de Antioquia, Diego Ospina for their suggestions throughout the research, Robinson Longas, Marta Sanchez, Andres Rivera and Amalia Betancur for their help and support. I also thanks to my future wife Mari Salinas and friends who have given me moral support in order to go through all the hard work.

Preface

This thesis is a compilation of my research done during my PhD time at Universidad de Antioquia. The main focus of research was the study of novel models that account for neutrino masses and mixing and provide a viable candidate for the DM in the Universe.

For the electroweak extension of the SM based on the $SU(3)_C \otimes SU(4)_L \otimes U(1)_X$ gauge group, several mechanisms for the neutrino mass generation through the tree-level realization of a dimension five Weinberg-like operator are proposed. For the so called model F, a three-family model, is found that the mixing matrix and mass hierarchy for the lightest neutrinos (the SM ones) and the exotic neutrinos (the heavy ones) turns out to be the same [1].

For the radiative type III seesaw model – a kind of scotogenic model – a collider study carried out in a simplify scenario, with scalar dark matter. Limits on the fermion triplet masses are set as a function of the flavor [2].

Contents

1. Introduction **3**

2. Standard Model and Beyond **9**

2.1. Standard Model . . . 9

2.1.1. Lagrangian . . . 10

2.1.2. Electroweak Symmetry Breaking . . . 11

2.1.3. SM shortcomings . . . 12

2.2. Minimal models for Neutrino mixing and masses . . . 13

2.2.1. Seesaw mechanism . . . 14

2.2.2. Type I/III Seesaw . . . 16

2.2.3. Type II Seesaw . . . 18

2.3. Radiative Models . . . 19

2.3.1. The Zee Model . . . 19

2.3.2. The Babu model . . . 20

2.3.3. The Ma Model . . . 21

3. Neutrino masses in the $SU(4)_L \otimes U(1)_X$ electroweak extension of the standard model **23**

3.1. $SU(4)_L \otimes U(1)_X$ models . . . 23

3.2. Dimension 5 effective operator . . . 25

3.2.1. Model A . . . 27

3.2.2. Model B . . . 28

3.2.3. Model E . . . 28

3.2.4. Model F . . . 29

3.3. Neutrino masses in Model F . . . 29

3.3.1. Canonical Seesaw Mechanism . . . 30

3.3.2. Type II-like Seesaw Mechanism . . . 32

4. Radiative Type III seesaw and its colliders phenomenology 37
4.1. The model . . . 37
4.1.1. Lagrangian . . . 38
4.1.2. Neutrino Mass Generation . . . 40
4.1.3. Lepton Flavor Violation (LFV) . . . 41
4.1.4. Dark matter . . . 42
4.2. Model Constraints . . . 43
4.2.1. Theory constraints . . . 43
4.2.2. Electroweak precision observables . . . 43
4.2.3. Collider constraints . . . 43
4.2.4. Flavor constraints . . . 45
4.2.5. Dark Matter constraints . . . 45
4.3. Scalar sector . . . 46
4.4. Phenomenology . . . 51
4.5. Collider limits . . . 54
4.6. Combination strategy . . . 56
4.7. Implementation of the model in Heptools . . . 56
4.8. Numerical results . . . 57
4.9. Best case scenario . . . 58
4.10. Worst case scenario . . . 61

5. Conclusions 63

A. CL$_s$ method 67

Bibliography 71

List of Figures 79

List of Tables 83

Chapter 1.

Introduction

"A person who never made a mistake never tried anything new"
— Albert Einstein

The standard model (SM) of particle physics remains as one of the most successful theories in Nature. It describes the fundamental interactions (strong and electroweak) of elementary particles. Despite its triumph, there are both theoretical and experimental reasons that suggest it is not the ultimate theory. From one side, the solar, atmospheric and reactor experiments have shown outstanding evidences supporting the neutrino oscillation phenomena [3–6], implying that neutrinos are massive particles. On the other hand, the hypothetical presence of an *invisible matter* which do not interact with visible matter, the so-called dark matter (DM), in the Universe has been indirectly known since the observations of galaxy rotation curves in the coma cluster made by F. Zwicky [7]. These two experimental facts are direct evidences that the SM is incomplete, and need to be extended. In addition to the neutrino problem and the DM issue, shortcomings such as the replications of fermions in Nature (why three families?), the observed matter-antimatter asymmetry in the Universe, fermion masses hierarchies, and the fact that quadratically divergent corrections to the Higgs boson mass m_H^2 destabilize the electroweak scale (naturalness problem), remains as puzzles to be solved.

The understanding of the physics behind neutrino masses and mixing is currently one of the major focus of research in particle physics today. Among the solutions to the neutrino problem, one of the simplest is given by the tree level realization of the Weinberg operator in the SM [8], which gives rise to the well-known type-I [9, 10], type-II [11–14] and type-III [15] seesaw mechanism, in where, an $SU(2)$ –fermion singlet, scalar triplet

and fermion triplet– are added respectively. The seesaw models are being explored at the large hadron collider (LHC) [16–21], with exception of the type-I seesaw, in where, due to the small production cross-section of singlet fermions, makes it difficult to probe it experimentally.

In order to explain the theoretical and phenomenological inconsistencies of the SM, its gauge group can also be extended. By extending its color group, and considering $SU(3)_C$ as a low-energy remnant symmetry of a larger group G_C, in Ref. [22] it was shown that in order to reproduce the low-energy phenomenology [1], then, the only possible choices are $G_C = SU(k)$ for $k = 4, 5$. This extension potentially can account for DM as a baryon of $SU(k-3)$ [23]. The top quark forward-backward anomaly is explained within the framework of an extended color sector [24]. The other possibility relies in extend the electroweak gauge group, from $SU(2)_L \otimes U(1)_Y$ to $SU(N)_L \otimes U(1)_X$ [25–29], for $N \in \{3, 4\}$. In this extension, the $SU(2)_L$ is enlarged to $SU(N)_L$. The new fermion content is accommodated into different fundamental representations, N or $\overline{N}$ of $SU(N)_L$. From a theoretical point of view, such extension can account for the number fermion generations in nature, when the anomaly cancellation takes place between families and not family by family as in the SM [28, 29]. When $N = 3$, we end up in the well-known 331 models. Since such models are a carbon copy of the SM, then neutrinos are also massless. Neutrino masses and mixing has been discussed in 331 models through the implementation of a type-I like seesaw [30] and the type-II like seesaw mechanism, in where an additional $SU(3)_L$ scalar sextet is added the 331 particle content [31–33]. These two seesaws arises from the tree level realization of a Weinberg-like operator. To our knowledge the type-III like seesaw which should correspond to the introduction of an $SU(3)_L$ fermion octet has not been study in the literature. For the electroweak extensions based on $SU(N)_L \otimes U(1)_X$ there is not a systematic classification of the realizations of the Weinberg operator, neither at the tree level or the loop level, reported in the literature so far. We carry out a systematic classification of the tree level realization of Weinberg-like operators that can explain neutrino masses in mixing in the electroweak extension of the SM based on the $SU(3)_C \otimes SU(4)_L \otimes U(1)_X$ [25–29] (341 extension for short) gauge group. The 341 gauge extension provides an explanation for the charge quantization [34], allows electroweak unification [27], can account for the muon anomalus magnetic moment [35, 36] and also arises in some little higgs models [37]. In this extension, neutrinos are massless, and a mechanism for neutrino mass generation is explored through non-renormalizable dimension five operator (Weinberg-like operator). For one of the

[1] Assuming that G_C is a simple group which breaks down to $SU(3)_C$ by introducing only one colored Higgs decuplet.

three-family models [2], the so-called model F, in where, besides the known neutrino, there is an additional neutral lepton in the lepton multiplet, we explain neutrino masses and mixing through a type I-like seesaw mechanism and a type II-like seesaw mechanism. For the latter case, after extending model F with a scalar decuplet, and imposing hierarchies in the vacuum expectation values (VEVs) of its neutral directions[3], the model predicts that the additional neutral leptons and the lightest SM neutrinos have the same mixing matrix and mass hierarchy. This model has tree level lepton flavor violation (LFV) processes, being $\mu \to 3e$ the most restrictive, induced by the doubly charged scalar H_1^{++} and controlled by its Yukawa coupling to the fermion sector, $y_{\alpha\beta}$. The one-loop realization of the Weinberg-like operator in the $SU(N)_L \otimes U(1)_X$ electroweak extension of the SM has not been explored in a systematic way. However, some implementations already exist, for instance, in the simplest little higgs model based on 331 gauge symmetry there exist a mechanism to explain the neutrino masses and mixing through the one-loop level realization of a Weinberg-like operator [39–41].

In the SM, the Weinberg operator has been explored systematically at the tree level (the seesaw mechanisms mentioned above), the one-loop level [42] and the two-loop level [43], such realization gives rise to an infinite set of models that can account for neutrino masses and mixing. For the one-loop models, after imposing a conserved $\mathbf{Z}_2$ discrete symmetry, and demanding that the particles propagating inside the loop transforms non-trivially under $\mathbf{Z}_2$, and the SM model particles transforms trivially under the same discrete symmetry, then a finite set of models that can account for both DM and neutrino masses arise [44]. Among the set of models, the radiative type III seesaw model (RSIII) [45, 46], in where in addition to the SM particle content, a $\mathbf{Z}_2$-odd scalar doublet and at least two $SU(2)_L$ $\mathbf{Z}_2$-odd fermion triplet are added. Since $\mathbf{Z}_2$ is conserved, then the lightest neutral $\mathbf{Z}_2$ particle (LOP) is the DM candidate. When the fermion triplet is the lightest $\mathbf{Z}_2$-odd state, and therefore, their neutral component the DM candidate, it turns out that in order to account for the observed relic density the fermion triplet must be very massive ~ 2.6 GeV [46]. In this scenario, the model can not be tested at the LHC. We study the scenario when the DM is the lightest neutral component of the scalar doublet. A collider analysis of the RSIII is carry out in a scenario with scalar DM, being the neutral component of the fermion triplet the next to the lightest $\mathbf{Z}_2$-odd particle (NLOP). The $\mathbf{Z}_2$-odd fermion may be light enough to be produced at the

[2] A model in which the number of fermion generations in nature is explained through the cancellation of chiral anomalies between families.

[3] Which is done in order to avoid larger mixing between the charged fermions in each multiplet and satisfy the SM ρ parameter constraint [38].

LHC. This motivates analyses designed to constrain the RSIII in present LHC searches and to potentially test their existence in the near future. For suitable choices of the spectrum, the new Yukawa interactions lead to the decay of the $\mathbf{Z}_2$-odd fermions, opening the possibility to generate collider signals of dileptons plus missing transverse energy (MET). The RSIII can explain the neutrino masses and mixing and account for the DM relic density. One of its main features is the richer collider phenomenology with strong similarities with the minimal supersymmetric standard model (MSSM) [47–49]. The decays of both, RSIII fermion triplets and supersymmetric particles are constrained by the $\mathbf{Z}_2$ symmetry, which leads to cascades to the lightest odd particle (LOP), given rise to a MET signature. In the framework of simplified model searches at the LHC, limits for sleptons and electroweakinos in the MSSM have been given for different spectra, characterized by sleptons being either lighter or heavier than the wino-like charginos and neutralinos [50–54]. The flavor of the decay leptons is determined by the new physics (NP) Yukawa couplings, which are related to the neutrino mass operators constrained by neutrino experiments [55]. A determination of the flavor structure of the final state is therefore highly relevant. The package `CheckMATE` [56–58] allows to obtain exclusion limits on supersymmetric simplified models and NP models based on an increasing number of ATLAS and CMS analyses. We analyze the exclusion sensitivity as a function of the flavor space, which is determined by new Yukawa couplings between the $\mathbf{Z}_2$-odd fields and the leptons. Decays with taus in the final state have a much lower exclusion sensitivity. Currently, only upper limits on stau production cross-sections have been reported by dedicated analyses for stau production by ATLAS [54] and CMS [59]. However, taking into account the larger cross-section for pairs of fermion triplets and recasting those results accordingly may allow to exclude light fermions decaying exclusively into taus and MET above the LEP exclusion limit [60] up to a lower mass limit of roughly 400 GeV, which allows to establish solid exclusion bounds within the RSIII and full flavor space allowed by neutrino physics, since final states with taus have the lowest exclusion sensitivity.

This thesis is organized as follows. In chapter 2 and introduction to the SM and theories for neutrino masses are reviewed. In chapter 3 a novel mechanism for neutrino mass generation in the 341 electroweak extension is introduced. In section 3.1, the 341 electroweak extension is reviewed, in the section 3.2 we classified the set of non-renormalizable effective operator in different models of the 341 extension. A mechanism for neutrino mass generation in the model F is explore through seesaw-like mechanism in the section 3.3. In chapter 4 the collider phenomenology for the RSIII is explored. The model is presented in section 4.1 Constraints on the model and their implications for the

low DM mass region are analyzed in section 4.2. In section 4.4 the collider phenomenology and the strategy to set limits on the RSIII is discussed. Numerical results are displayed in section 4.8 . Finally we summarize our main results in section 5.

Chapter 2.

Standard Model and Beyond

2.1. Standard Model

The strong, electromagnetic and weak interaction in the SM are described by the $G_{\text{SM}} = SU(3)_C \otimes SU(2)_L \otimes U(1)_Y$ gauge symmetry. Meaning that its lagrangian is invariant under local transformation of G_{SM}. So far, it is the most compelling and successful theory in science since its predictions are being confirmed with huge precision in many different experiments. The particle content of the SM is displayed in table 2.1, grouped into matter particles and force mediator particles. The matter particles are spin one-half particles (fermions), which are classified into quarks and leptons. In total there are three generations of matter particles in nature. The first generation of matter particles are the building blocks of the atoms. The second and third generation are replications of the first one, but the particles are heavier, and as they decay too quickly then, they do not form stable bound states. The interactions on the SM are mediated by the spin one particles (the gauge bosons). All the quarks carry colour charge (red, green, blue) and interact through the strong force mediated by the gluons. There are in total eight gluons and they transform as an octet under the color group $SU(3)_C$. The up-type quarks and the down-type quarks carry an electric charge of $+2/3e$ and $-1/3e$ respectively. The charged leptons carry electric charge $-1e$. All electrical charged particle interact through the electromagnetic force mediated by massless photons with no electric charge. Each charged lepton have an electrical neutral partner (the neutrino). All the particles interact through the weak force, which is mediated by the electrically charge $W^{\pm}$ and the neutral Z vector bosons.

		$(\mathrm{SU}(3)_C, SU(2)_L, U(1)_Y)$	$\mathrm{U}(1)_Q$
Quarks	$Q_L^\alpha = \begin{pmatrix} u^\alpha \\ d^\alpha \end{pmatrix}_L$	$(\mathbf{3}, \mathbf{2}, 1/3)$	$\begin{pmatrix} 2/3 \\ -1/3 \end{pmatrix}$
	u_R^α	$(\bar{\mathbf{3}}, \mathbf{1}, 4/3)$	$2/3$
	d_R^α	$(\bar{\mathbf{3}}, \mathbf{1}, 2/3)$	$-1/3$
Leptons	$L_L^\alpha = \begin{pmatrix} \nu^\alpha \\ l^\alpha \end{pmatrix}_L$	$(\mathbf{1}, \mathbf{2}, -1)$	$\begin{pmatrix} 0 \\ -1 \end{pmatrix}$
	l_R^α	$(\mathbf{1}, \mathbf{1}, -2)$	-1
Higgs	$\mathrm{H}=\begin{pmatrix} H_1^+ \\ H_1^0 \end{pmatrix}$	(1,2,1)	$\begin{pmatrix} 1 \\ 0 \end{pmatrix}$
Gauge bosons	G_μ^α	$(\mathbf{8}, \mathbf{1}, 0)$	0
	W_μ^i	$(\mathbf{1}, \mathbf{3}, 0)$	$(0, \pm 1)$
	B_μ	$(\mathbf{1}, \mathbf{1}, 0)$	0

Table 2.1.: The particle content of the SM. The generation index is represented by α and each up-type quark u^α and down-type one d^α, carries also color charge.

In the SM, the electroweak sector $SU(2)_L \otimes U(1)_Y$ of G_{SM} is a broken symmetry. When a fundamental scalar transforming as a doublet under $SU(2)$ develops a vacuum expectation value (VEV) it triggers the spontaneous symmetry breaking. After $SU(2)_L \otimes U(1)_Y$ is broken a remnant symmetry $U(1)_Q$ of electromagnetism remains as an exact symmetry in nature.

2.1.1. Lagrangian

The most general renormalizable lagrangian reads:

$$\begin{aligned} \mathcal{L} &= -\frac{1}{4} F_{\mu\nu}^\alpha F^{\mu\nu\alpha} + \left\{ i\overline{\Psi}\gamma^\mu D_\mu \Psi + h.c. \right\} \\ &+ \left\{ \overline{\Psi} Y \Phi H + h.c. \right\} + |D_\mu H|^2 - V(H). \end{aligned} \tag{2.1}$$

In Eq. (2.1), the first term in the first line is the kinetic term for the gauge sector of the electroweak theory, where α runs over the total number of gauge bosons. Their

field-strength tensors are given by:

$$\begin{aligned} F^i_{\mu\nu} &= \partial_\mu W^i_\nu - \partial_\nu W^i_\mu + g\epsilon_{jki} W^j_\mu W^k_\nu \\ f_{\mu\nu} &= \partial_\mu B_\nu - \partial_\nu B_\mu, \end{aligned} \tag{2.2}$$

In Eq. (2.2), g is the coupling constant associated to $SU(2)_L$ and ϵ_{jki} its structure constant.

The second part in the first line of Eq. (2.1) is the Dirac lagrangian, it describes the interactions between matter fields Ψ and the gauge boson fields. The first part in the second line of Eq. (2.1) is the yukawa sector, it describes the interactions between matter fields Ψ and the Higgs field H. This part of the lagrangian is the responsible for masses of the fermions which take place when the electroweak symmetry breaking occurs. The last part in Eq. (2.1) is the scalar sector, which splits into a kinetic term and a potential term, and is responsible for the triggering the electroweak symmetry breaking (EWSB). The covariant derivative D_μ, which appears in the Dirac sector and the Higgs sector is given by:

$$D_\mu = \partial_\mu + \frac{ig'}{2} B_\mu Y + \frac{ig}{2} \tau^l W^l_\mu, \tag{2.3}$$

with g' being the gauge coupling associated to $U(1)_Y$, τ^l the set of Pauli matrices, for $l = 1, 2, 3$, which are proportional to the generators of $SU(2)_L$ and Y the $U(1)_Y$ hypercharge generator.

2.1.2. Electroweak Symmetry Breaking

In the lagrangian in Eq. (2.1), all the fermions and force carriers are massless. A mass term for the fermion, such as $\mathcal{L} = m\overline{\Psi}\Psi$ breaks the lagrangian invariance under G_{SM}. Experimentally, fermions and gauge bosons have masses. The way in which their masses are generated without spoiling the renormalizability of the theory is through the Higgs mechanism. A scalar doublet H under $SU(2)_L$ is added to the fundamental lagrangian (last term in Eq. (2.1)). The scalar sector of the lagrangian is:

$$\begin{aligned} \mathcal{L}_{\text{scalar}} &= |D_\mu H|^2 - V(H). \\ &= \left| \left(\partial_\mu + \frac{ig'}{2} B_\mu Y + \frac{ig}{2} \tau^l W^l_\mu \right) H \right|^2 - \left[\mu^2 H^\dagger H + \lambda (H^\dagger H)^2 \right], \end{aligned} \tag{2.4}$$

where H, is expressed by:

$$H = \begin{pmatrix} G^+ \\ \frac{1}{\sqrt{2}}(v + h + iG_I^0) \end{pmatrix}, \tag{2.5}$$

After the Higgs develops a non-zero vacuum expectation value (VEV), G^+ and G_I^0 are Goldstone bosons which becomes in the longitudinal degrees of freedom of the W^+ and the Z boson respectively.

$$\langle H \rangle = \begin{pmatrix} 0 \\ \frac{v}{\sqrt{2}} \end{pmatrix}, \tag{2.6}$$

with $v = 246$ GeV.

The masses for the fermions are obtained from the yukawa lagrangian once the Higgs acquieres a non zero VEV. And the masses for the fermions are proportional to the v. And from the kinetic term of the scalar lagrangian arises in a natural way masses for the force mediator, the W^+ and Z gauge bosons. The photon remains massless.

2.1.3. SM shortcomings

The SM is not expected to be the final description of the fundamental interactions, but is an effective low-energy manifestation of a more fundamental theory.

- The SM does not incorporate gravitation. A theory which is describe at classical level by the general theory of relativity. One of the greatest challenges of building a quantum field theory of gravity is its non-renormalizability. Loop quantum gravity [61] and string theories [62] stands as attempts to build a quantized theory of gravity.
- The observed baryon-antibaryon asymmetry can not be explained within the context of the SM. Physics beyond the SM is require in order to provide an explanation to the observed phenomena. One possible solution lies in leptogenesis scenarios, in where the baryon-antibaryon asymmetry is explained through a lepton asymmetry generated by decays of heavy sterile neutrinos [63].

- The observation of galaxy rotation curves can not be explained within the context of the known physics. It can be explained by postulating the existence of a new type of weakly interacting matter, the so-called dark matter [7].
- There are not a theoretical explanation for the mass hierarchy of known fermions.
- Neutrino mixing and masses are not explain within the framework of the SM. Therefore a mechanism for neutrino masses is require.

2.2. Minimal models for Neutrino mixing and masses

In the SM neutrinos are massless due to the absence of right-handed (RH) neutrinos ν_R. However, if RH neutrinos (as well as left-handed (LH) antineutrinos $\overline{\nu}_R$) exist in nature, their interaction with matter should be much weaker than the weak interaction of left-handed neutrinos. As a consequence, they must transform as a singlet under G_{SM} gauge group. And should have not gauge interaction[1]. If in addition to the SM particle content it is assumed the existence of hypothetical new fields (right-handed neutrinos, a 4th generation of fermions, new scalars *e*tc.), these could play a crucial role in the neutrino mass generation.

For any Dirac particle ψ, a mass term is given by [64]:

$$\begin{aligned} -\mathcal{L}^{D}_{\text{Mass}} &= m\overline{\psi}\psi \\ &= m(\overline{\psi}_L\psi_R + \overline{\psi}_R\psi_L), \end{aligned} \tag{2.7}$$

where the relation $\psi = \psi_L + \psi_R$, has been used. However, such a term is not invariant under G_{SM}, and therefore forbidden in the fundamental lagrangian. The SM relies in the Higgs Mechanism [64] to explain the way as the particles obtain their masses. All known fermions (except neutrinos) acquire masses after the EWSB takes place:

$$SU(3)_C \otimes SU(2)_L \otimes U(1)_Y \overset{v\sim 246\,\text{GeV}}{\longrightarrow} SU(3)_C \otimes U(1)_Q. \tag{2.8}$$

[1] They not couple to the weak $W^{\pm}$, Z^0, gluons and photon bosons.

The interaction between fermions and the fundamental scalar, known as the yukawa interaction is described by the lagrangian:

$$-\mathcal{L}_{\text{Yuk}} = \lambda \overline{\psi}_R H^\dagger \psi_L + h.c, \tag{2.9}$$

being λ the yukawa coupling that measures the strength of the interaction between the scalar and the fermion. When the Higgs acquire a VEV, $\langle H \rangle = v/\sqrt{2}$, the yukawa lagrangian takes the form:

$$-\mathcal{L}_{Yuk} = \lambda \frac{v}{\sqrt{2}} \overline{\psi}_R \psi_L + h.c, \tag{2.10}$$

Comparing Eq. (2.7) with Eq. (2.10), we find that after the EWSB, the fermion ψ acquire a mass: $m_D = (\lambda v)/\sqrt{2}$. However this mass term require the existence both of the right-handed and the left-handed components of the fermion field ψ. This mass term is called a *D*irac mass term. Many extensions of the SM provides an answer to the neutrino puzzle as well as many other shortcomings (electroweak hierarchy problem, dark matter, gauge couplings unification, *etc.*) just by extending either the fermion or the scalar particle content. Since a Majorana, ψ, particle can be its own antiparticle, it must have zero electric charge. This implies that $\psi^c = \psi$ (with c standing for the charge conjugation operator), where the phase term has been neglected. The Eq. (2.7) for a Majorana field looks like:

$$-\mathcal{L}^M_{Mass} = \frac{1}{2} m \overline{\psi^c} \psi + h.c., \tag{2.11}$$

this is called a *M*ajorana mass term. At this stage, neutrinos can be either Dirac or Majorana particles. In order to explain neutrino masses, it is necessary go beyond the SM. In the next sections we review several mechanisms widely studied, which allow neutrinos to be massive particles.

2.2.1. Seesaw mechanism

The first attempt to explain the neutrino mixing and masses relies in the idea of extend the SM particle content adding a RH neutrino N_R per lepton generation [9]. The yukawa lagrangian involving the usual LH doublet $L_L = (\nu_L, l_L)^T$, the scalar field $H = (H_1^+, H_1^0)^T$ and the new RH neutrino is expressed by:

$$-\mathcal{L}_{\text{Yuk}} = \lambda \overline{L}_L \widetilde{H} N_R + h.c, \tag{2.12}$$

where $\widetilde{H} = i\tau_2 H^*$ (being τ_2 the second Pauli matrix). After the EWSB, Eq. (2.12) leads to a Dirac mass term

$$-\mathcal{L}^{D}_{\text{Mass}} = \overline{\nu}_L m_D N_R + h.c, \tag{2.13}$$

with $m_D = \lambda v/\sqrt{2}$. However, a Majorana mass term for N_R can also be added,

$$-\mathcal{L}^{M}_{Mass} = \frac{1}{2}\overline{N^c_R} m_R N_R + h.c.. \tag{2.14}$$

Denoting $n_L = (\nu_L, N^c_R)^T$, the full lagrangian is written as

$$\begin{aligned} \mathcal{L}_{Mass} &= \mathcal{L}^{M}_{Mass} + \mathcal{L}^{D}_{Mass} \\ &= \frac{1}{2}\overline{n^c_L} M n_L, \end{aligned} \tag{2.15}$$

where

$$M = \begin{pmatrix} 0 & m_D \\ m^T_D & m_R \end{pmatrix}. \tag{2.16}$$

After diagonalization.

$$m_{2,1} = \frac{1}{2}\Big(m_R \pm \sqrt{m^2_R + 4m^2_D}\Big). \tag{2.17}$$

With m_1 and m_2 the masses for the lightest neutrino and the heavy neutrino respectively. Demanding that m_1 to be comparable to the charged leptons masses, then, m_2 must be close to the GUT scale, $m_2 \sim 10^{15}$ GeV. In this mechanism, the smallness of neutrino masses is a consequence of the heaviness of the RH neutrinos. Such a mechanism is called *the type I seesaw mechanism*. There exist three realizations of the seesaw mechanism at tree-level [8] which are shown in Fig 2.1. These are based on the fact that two $SU(2)$ doublets can be decomposed into a singlet and a triplet ($\mathbf{2} \otimes \mathbf{2} = \mathbf{3} \oplus \mathbf{1}$).

The type I, type II and type III seesaw mechanism are the realizations of the dimension-five effective Weinberg operator at tree-level [8].

$$\mathcal{L}_\Lambda = \frac{1}{2} f_{\alpha\beta}\Big(\overline{L^c_{L\alpha}}\widetilde{H}^*\Big)\Big(\widetilde{H}^\dagger L_{L\beta}\Big) + h.c., \tag{2.18}$$

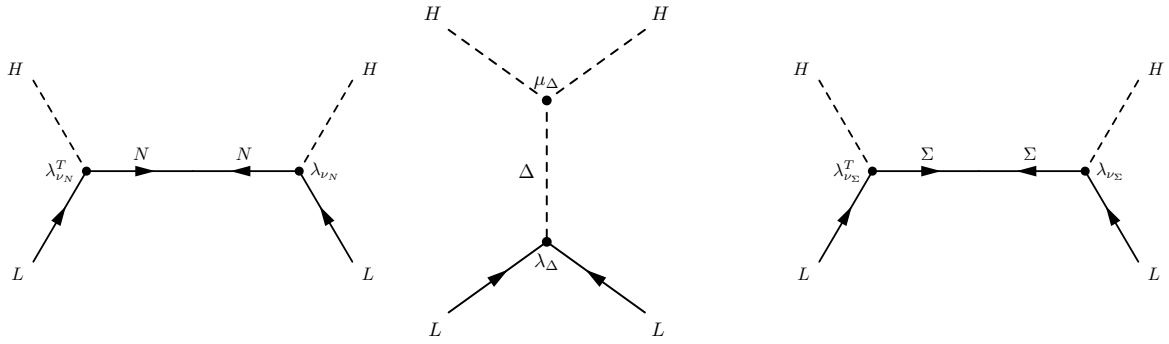

Figure 2.1.: realizations of the seesaw mechanism: Type I (left), Type II (in the middle) and Type III (right). The exchanged massive particle corresponds to a fermion singlet $N_R \sim (\mathbf{1}, \mathbf{1}, 0)$, a scalar triplet $\Delta \sim (\mathbf{1}, \mathbf{3}, -2)$ and a fermion triplet $\Sigma \sim (\mathbf{1}, \mathbf{3}, 0)$, respectively.

where $f_{\alpha\beta}$ is a coefficient suppressed by an energy scale Λ (associated to the existence of new heavy fields) and its calculation depends of the degree of realization of the operator (depending whether the realization is either at tree-level or at loop-level).

In what follows, the seesaw realizations are briefly introduced.

2.2.2. Type I/III Seesaw

Following the Eq. (2.18),

$$\mathcal{L}_\Lambda = \frac{1}{2} f_{\alpha\beta} \left(\overline{L^c_{L\alpha}} \widetilde{H}^* \right) \left(\widetilde{H}^\dagger L_{L\beta} \right) + h.c.. \tag{2.19}$$

after the EWSB, the Higgs field acquires a non-zero VEV: $\langle H \rangle = v/\sqrt{2}$, and the Weinberg operator takes the form:

$$\mathcal{L}_\Lambda = \frac{1}{2} (\mathcal{M}_\nu)_{\alpha\beta} \overline{\nu^c_L} \nu_L, \tag{2.20}$$

with

$$(\mathcal{M}_\nu)_{\alpha\beta} = f_{\alpha\beta} v^2, \tag{2.21}$$

that is, a Majorana mass. A simple evaluation shows that, in order to obtain $m_\nu < 1$ eV, then $(f_{\alpha\beta})^{-1} > 10^{15}$ GeV. However, what is $f_{\alpha\beta}$?; with the aim of giving an answer, let

us considerer the most general yukawa lagrangian already written in Eq. (2.15) for the type I seesaw.

$$-\mathcal{L}_{yuk} = \lambda \overline{L}_L \widetilde{H} N_R + \frac{1}{2}\overline{N_R^c} m_R N_R + h.c. \tag{2.22}$$

After the EWSB, and in matrix form:

$$-\mathcal{L}_{yuk} = \frac{1}{2}\begin{pmatrix}\overline{\nu_L} & \overline{N_R^c}\end{pmatrix}\begin{pmatrix}0 & m_D \\ m_D^T & m_R\end{pmatrix}\begin{pmatrix}\nu_L^c \\ N_R\end{pmatrix} + h.c. \tag{2.23}$$

Now if $m_D << m_R$, by block diagonalization we obtain:

$$\begin{aligned}\mathcal{M}_{\nu_L} &\simeq -m_D m_R^{-1} m_D^T, \\ \mathcal{M}_{N_R} &\simeq m_R.\end{aligned} \tag{2.24}$$

From Eq. (2.21) and Eq. (2.24), we find that $f_{\alpha\beta}$ has the form:

$$f_{\alpha\beta} = -\frac{1}{2}\frac{\lambda\lambda^T}{m_R}, \tag{2.25}$$

It is found that in order to obtain $M_{\nu L} \sim 1$ eV, then $m_R \sim 10^{15}$ GeV for yukawa couplings $\mathcal{O}(\lambda) \sim 1$. The same procedure should be done for the type III seesaw. By introducing a fermion triplet $\Sigma_R \sim (\mathbf{1}, \mathbf{3}, 0)$ to the SM particle content, the most general yukawa lagrangian involving Σ_R and the neutrino takes the form:

$$-\mathcal{L}_{yuk} = \overline{L}_L \lambda_\Sigma \big(\overrightarrow{\Sigma}.\overrightarrow{\tau}\big)\widetilde{H} + \frac{1}{2}\overline{\overrightarrow{\Sigma^c}} m_\Sigma \overrightarrow{\Sigma} + h.c. \tag{2.26}$$

After the EWSB, the previous equation yields:

$$-\mathcal{L}_{yuk} = \frac{1}{2}\begin{pmatrix}\overline{\nu_L} & \overline{\Sigma_3^c}\end{pmatrix}\begin{pmatrix}0 & m_D \\ m_D^T & m_{\Sigma_3}\end{pmatrix}\begin{pmatrix}\nu_L^c \\ \Sigma_3\end{pmatrix} + h.c., \tag{2.27}$$

with $\overrightarrow{\Sigma} = (\Sigma_1, \Sigma_2, \Sigma_3)$. This mechanism leads to the same result obtained for the type I seesaw after the mass matrix is block diagonalized. Besides, adding a fermion triplet instead a fermion singlet, yields additional phenomenology. For instance, LFV processes like $\Sigma^\pm \to l^\pm \nu$.

2.2.3. Type II Seesaw

Adding a scalar triplet $\Delta \sim (\mathbf{1}, \mathbf{3}, 2)$, to the SM particle content:

$$\Delta = \begin{pmatrix} \Delta^+/\sqrt{2} & \Delta^{++} \\ \Delta_0 & -\Delta^+/\sqrt{2} \end{pmatrix}, \tag{2.28}$$

the relevant lagrangian is written as:

$$-\mathcal{L}_\Delta = \left(\widetilde{\overline{L}}_L \lambda_\Delta \Delta L_L + h.c.\right) + V(H, \Delta), \tag{2.29}$$

with

$$V(H, \Delta) = m_\Delta^2 tr\{\Delta\Delta^\dagger\} + (\mu_\Delta \widetilde{H}^\dagger \Delta^\dagger H + h.c.). \tag{2.30}$$

In order to guarantee lepton number (LN) conservation in Eq. (2.29), we assign LN $= -2$ to Δ, but this implies the LN is violated explicitly by the μ term in Eq. (2.30). After the EWSB, and allowing to the scalar triplet to develop a non-vanishing VEV in the neutral direction $\langle\Delta\rangle = v_\Delta$, the term relevant for neutrino masses given in Eq. (2.29) acquires the form:

$$-\mathcal{L}_{\text{Mass}} = \lambda_\Delta v_\Delta \overline{\nu_L^c} \nu_L, \tag{2.31}$$

then

$$\mathcal{M}_\nu = 2\lambda_\Delta v_\Delta. \tag{2.32}$$

From Eq. (2.30), after the two scalars acquire a non-zero VEV and ensuring a minimum value for $V(H, \Delta)$ is reach.

$$v_\Delta = -\frac{\mu_\Delta v^2}{4m_\Delta^2}, \quad n\text{for} \quad m_\Delta >> m_H. \tag{2.33}$$

Taking into account the two previous equations, the expression for the neutrino mass looks like

$$\mathcal{M}_\nu = -\frac{\lambda_\Delta \mu_\Delta v^2}{2m_\Delta^2}, \tag{2.34}$$

Making a comparison between this result and the outcome from the effective dimension-five operator in Eq. (2.18) we obtain,

$$f_{\alpha\beta} = -\frac{\lambda_\Delta \mu_\Delta}{m_\Delta^2}. \tag{2.35}$$

The type II seesaw has a very rich phenomenology. The existence of the new field Δ, still undiscovered, modifies the ρ parameter of the SM putting a strong constraint on the VEV of this new scalar: $v_\Delta \leq 3$ GeV [65]. An interesting feature of this seesaw is that leads to LFV processes in the charged sector such as $\mu \to e\gamma$, $\tau \to \mu\gamma$. In the next section we provided a very brief introduction to some models in which neutrino obtain their masses radiatively.

2.3. Radiative Models

In the SM, the charged fermions acquire mass through yukawa interaction, in which the Higgs boson plays a crucial role, after the EWSB takes place, however, the neutrino remains massless in the SM. The type I seesaw mechanisms discussed previously lead naturally to a massive neutrino by the introduction of heavy fields (at the GUT scale) with masses around 10^{15} GeV, making these theories very difficult (with rare decays under special conditions) to be tested in colliders. Neutrino masses, however, could be originated from a radiative mechanism.

2.3.1. The Zee Model

In order to explain the origin of the neutrino mixing and masses is given by the Zee model [66], in which the masses are generated at one-loop order. In this model, in addition to the Higgs field H, two additional scalar fields $\phi \sim (\mathbf{1}, \mathbf{2}, 1)$ and $\chi^{(+)} \sim (\mathbf{1}, \mathbf{1}, 2)$ are added to the SM particle content. The relevant lagrangian of the Zee model is:

$$\mathcal{L}_{\text{Zee}} = \overline{\widetilde{L}_{L\alpha}} h_{\alpha\beta} L_{L\beta} \chi^{(+)} + \mu \chi^{(+)} H^\dagger \widetilde{\phi} + h.c., \tag{2.36}$$

where only H couples to leptons. In order to ensure LN conservation in the yukawa sector, the $\chi^{(+)}$ carries lepton number -2. The coupling $h_{\alpha\beta}$ is antisymmetric due to the Fermi-Dirac statistic. This latter feature implies a neutrino mass matrix with zeros in its diagonal entries. Making one species of neutrino massless. The Zee model allows

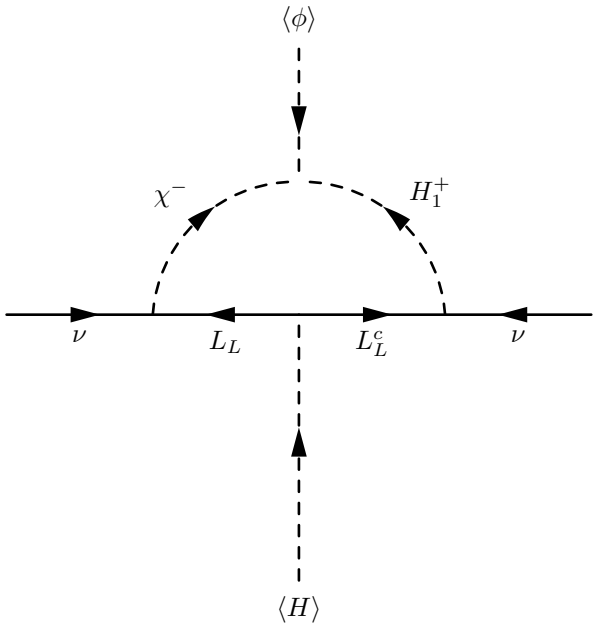

Figure 2.2.: One-loop diagram in the Zee model.

to generate Majorana mass for the neutrino at one-loop order. The relevant Feynman diagram is shown in Fig. 2.2. In this model the neutrino mass matrix has the form:

$$\mathcal{M}_\nu \sim \begin{pmatrix} 0 & h_{\mu e}(m_\mu^2 - m_e^2) & h_{\tau e}(m_\tau^2 - m_e^2) \\ h_{\mu e}(m_\mu^2 - m_e^2) & 0 & h_{\tau\mu}(m_\tau^2 - m_\mu^2) \\ h_{\tau e}(m_\tau^2 - m_e^2) & h_{\tau\mu}(m_\tau^2 - m_\mu^2) & 0 \end{pmatrix}. \tag{2.37}$$

This model lead to LFV processes such as $\mu \to e\gamma$, $\tau \to e\mu$. The original version of Zee model does not match with the experimental data: predicts a maximum value for the solar neutrino mixing angle $\theta_\odot(\theta_{12})$, and does not reproduce the spectrum of neutrino masses. For these reasons the simplest version of Zee model has been rule out [67].

2.3.2. The Babu model

In this model [68], an electrically charged scalar singlet $h^{(+)} \sim (\mathbf{1}, \mathbf{1}, 2)$ and a charged scalar doublet $k^{(++)} \sim (\mathbf{1}, \mathbf{1}, 4)$, are added to the SM particle content. The most general lagrangian associated with these new fields read:

$$\mathcal{L}_{\text{Babu}} = \left(\overline{L_{L\alpha}^c} f_{\alpha\beta} L_{L\beta} h^{(+)} + \overline{L_{R\alpha}^c} y_{\alpha\beta} L_{R\beta} k^{(++)} + h.c.\right) - V(H, h^+, k^{++}), \tag{2.38}$$

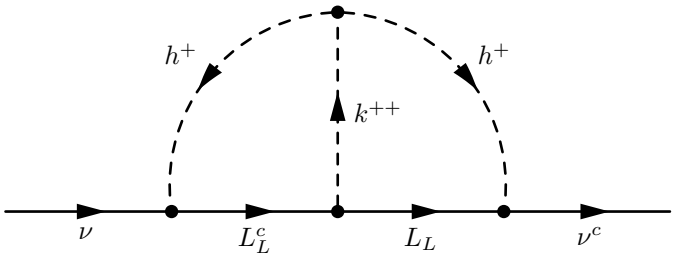

Figure 2.3.: Two-loop neutrino mass generation in the Babu model.

where the potential term in the scalar sector is given by:

$$V(H, h^+, k^{++}) \quad = \quad \mu h^- h^- k^{++} + h.c. \tag{2.39}$$

The coupling $f_{\alpha\beta}$ is antisymmetric. The trilinear interaction shown in Eq. (2.39) violates LN by two units. The contribution to the neutrino masses appear at the two-loop level as it is shown in Fig. 2.3. The neutrino mass matrix has the form:

$$\mathcal{M}_{\alpha\beta} \quad = \quad 8\mu f_{\alpha\gamma} y^{'}_{\gamma\delta} m_\gamma m_\delta \mathcal{I}_{\gamma\delta} (y^\dagger)_{\gamma\beta}, \tag{2.40}$$

with $y^{'}_{\alpha\beta} = \zeta y^{'}_{\alpha\beta}$, where $\zeta = 1$ for $\alpha = \beta$ and $\zeta = 2$ for $\alpha \neq \beta$, being $m_{(\gamma,\delta)}$ the charged lepton masses. The term $I_{\gamma\beta}$ is a two-loop integral

$$\mathcal{I}_{\gamma\delta} \quad = \quad \int \frac{d^4p}{(2\pi)^4} \int \frac{d^4q}{(2\pi)^4} \frac{1}{(p^2 - m_h^2)} \frac{1}{(p^2 - m_{\gamma}^2)} \frac{1}{(q^2 - m_h^2)} \frac{1}{(q^2 - m_{\delta}^2)} \frac{1}{(p-q)^2 - m_k^2} \tag{2.41}$$

This integral has been evaluated in Ref. [69]. Since $\det(\mathcal{M}_\nu) = 0$, the model and predicts one of the neutrinos to remain massless. The Babu model also leads to LFV processes such as $\mu \to eee$, $\tau \to \mu\mu\mu$ which occurs at tree-level via $k^{(++)}$ exchange.

2.3.3. The Ma Model

An interesting model that can account for neutrino mixing and masses and also provides a DM candidate in the universe is the so-called Radiative Seesaw [70]. In this model an extra discrete Z_2 symmetry is added, and a minimal particle extension : a hypothetical new scalar doublet and three right-handed neutrinos are added to the SM particle content. Under $SU(3)_C \otimes SU(2)_L \otimes U(1)_Y \otimes Z_2$, the new particle content transforms as:

$$\eta \quad = \quad (\eta^+, \eta^0)^T \sim (\mathbf{1}, \mathbf{2}, 1, -), \quad N_{R\alpha} \sim (\mathbf{1}, \mathbf{1}, 0, -), \tag{2.42}$$

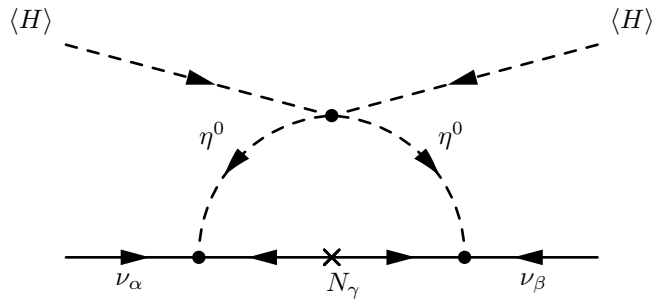

Figure 2.4.: One-loop neutrino mass generation in the Ma model.

.

The new particles $N_{R\alpha}$ and η are odd under Z_2. The remaining particles of the SM are even under Z_2. The relevant lagrangian reads:

$$\mathcal{L}_{\text{Ma}} = h_{\alpha\beta}(\nu_\alpha \eta^0 - l_\beta \eta^+) N_{R\beta} + \frac{1}{2}\overline{N^c_{R\alpha}} M_{R_{\alpha\beta}} N_{R\beta} + \frac{1}{2}\lambda_5 (H^\dagger \eta)^2 + h.c. \quad (2.43)$$

η can not develop a VEV and as a consequence Z_2 remains an unbroken symmetry. This model has a neutral lightest stable particle (LSP) which plays the role of the DM.

Tiny masses for the neutrinos are generated at one-loop level as it is shown in Fig. 2.4. The mass matrix takes the form:

$$(\mathcal{M}_\nu)_{\alpha\beta} = \sum_\gamma \frac{h_{\alpha\gamma} h_{\beta\gamma} M_\gamma}{16\pi^2} \left[\frac{m_R^2}{m_R^2 - M_\gamma^2} \ln\left(\frac{m_R^2}{M_\gamma^2}\right) - \frac{m_I^2}{m_I^2 - M_\gamma^2} \ln\left(\frac{m_I^2}{M_\gamma^2}\right) \right], \quad (2.44)$$

being m_R and m_I the masses of $\sqrt{2}Re(\eta^0)$ and $\sqrt{2}Im(\eta^0)$, respectively. The Ma model is testable at the LHC. Numerically, in order to have neutrino masses $m_\nu \sim 1$ eV and assuming a $\lambda_5 \sim 10^{-4}$ is found that $M_\gamma \sim 1$ TeV. On the other hand, there will be observable dacays[2] such as $\eta^{(\pm)} \to l^{(\pm)} N_{1,2,3}$.

[2] Assuming that the mass of the scalar fields are greater than M_γ.

Chapter 3.

Neutrino masses in the $SU(4)_L \otimes U(1)_X$ electroweak extension of the standard model

In this chapter we explore mechanisms for the neutrino mass generation in an electroweak extension of the standard model based on $SU(3)_C \otimes SU(4)_L \otimes U(1)_X$ gauge group.

3.1. $SU(4)_L \otimes U(1)_X$ models

In this section the 3-4-1 electroweak extension is briefly introduced. A full phenomenological study can be found in references [27, 28, 71]. We focus in the lepton sector, due that our aim is to implement higher dimensional effective operators that can account for the neutrino mass generation at the tree-level. In the electroweak $SU(4)_L \otimes U(1)_X$, the electric charge operator is a linear combination of the diagonal generators from the Cartan subalgebra [72, 73].

$$Q = aT_{3L} + \frac{b}{\sqrt{3}}T_{8L} + \frac{c}{\sqrt{6}}T_{15L} + XI_4, \tag{3.1}$$

where $a = 1$ is taken in order to reproduce the SM phenomenology. The T_{iL} are the generators of $SU(4)_L$, normalized as $Tr(T_iT_j) = \delta_{ij}/2$, X is the hypercharge and I_4 represents the 4×4 identity matrix. The coefficients b and c remain as free parameter that need to be chosen to obtain a model in particular. After demanding models that include particles without exotic electric charge [72], two different assignments for the

Table 3.1.: Particle content for models A and B, the $\alpha = \{1, 2, 3\}$ are the lepton generation indices, i run over the first two generations of quarks. The numbers in parentheses refer to the $(SU(3)_C, SU(4)_L, U(1)_X)$ quantum numbers respectively.

Model A	Model B
$L_{L\alpha} = (\ e^-,\ \ \nu^0,\ \ N^0,\ \ N'^0\ )_{L\alpha} \sim (1, \overline{4}, -1/4)$,	$L_{L\alpha} = (\ \nu^0, e^-\ ,\ \ E^-,\ \ E'^-\ )_{L\alpha} \sim (1, 4, -3/4)$,
$e^+_{L\alpha} \sim (1, 1, 1)$,	$e^+_{L\alpha} \sim (1, 1, 1)$, $E^+_{L\alpha} \sim (1, 1, 1)$, $E'^+_{L\alpha} \sim (1, 1, 1)$,
$Q_{iL} = (\ u_i,\ \ d_i,\ \ D_i,\ \ D'_i\ ) \sim (3, 4, -1/12)$,	$Q_{iL} = (\ d_i,\ \ u_i,\ \ U_i,\ \ U'_i\ ) \sim (3, \overline{4}, 5/12)$,
$u^c_{iL} \sim (\overline{3}, 1, -2/3), d^c_{iL} \sim (\overline{3}, 1, 1/3)$,	$u^c_{iL} \sim (\overline{3}, 1, -2/3), d^c_{iL} \sim (\overline{3}, 1, 1/3)$,
$D^c_{iL} \sim (\overline{3}, 1, 1/3), D'^c_{iL} \sim (\overline{3}, 1, 1/3)$,	$U^c_{iL} \sim (\overline{3}, 1, -2/3), U'^c_{iL} \sim (\overline{3}, 1, -2/3)$,
$Q_{3L} = (\ d_3,\ \ u_3,\ \ U_3,\ \ U'_3\ ) \sim (3, \overline{4}, 5/12)$,	$Q_{3L} = (\ u_3,\ \ d_3,\ \ D_3,\ \ D'_3\ ) \sim (3, 4, -1/12)$,
$u^c_{3L} \sim (\overline{3}, 1, -2/3), d^c_{3L} \sim (\overline{3}, 1, 1/3)$,	$u^c_{3L} \sim (\overline{3}, 1, -2/3), d^c_{3L} \sim (\overline{3}, 1, 1/3)$,
$U^c_{3L} \sim (\overline{3}, 1, -2/3), U'^c_{3L} \sim (\overline{3}, 1, -2/3)$,	$D^c_{3L} \sim (\overline{3}, 1, 1/3), U'^c_{3L} \sim (\overline{3}, 1, 1/3)$,

free parameters are allowed. The first one, based on the selection of $b = 1$ (-1) and $c = 1$ (-1) which gives rise to two three-family models, Model A and Model B, and the other choice for the free parameters is $b = 1$ (-1) and $c = -2$ (2) that also gives rise to two three-family models, Model E and Model F[1].

The electroweak gauge boson sector are contained in the $SU(4)_L$ adjoint representation. There are a total of 15 of them, which can be written as:

$$\frac{1}{2}\lambda_\alpha A^\alpha_\mu = \begin{pmatrix} D^0_{1\mu} & W^+_\mu & K^{(b+1)/2}_\mu & X^{(3+b+2c)/6}_\mu \\ W^-_\mu & D^0_{2\mu} & K^{(b-1)/2}_{1\mu} & V^{(-3+b+2c)/6}_\mu \\ K^{-(b+1)/2}_\mu & K^{-(b-1)/2}_{1\mu} & D^0_{3\mu} & Y^{-(b-c)/3}_\mu \\ X^{-(3+b+2c)/6}_\mu & V^{(3-b-2c)/6}_\mu & Y^{(b-c)/3}_\mu & D^0_{4\mu} \end{pmatrix} . \tag{3.2}$$

The Model A and Model B are displayed in table 3.1. The scalar sector for this set of models is given by:

$$\begin{aligned} \langle \Phi^T_1 \rangle &= \langle (\phi^0_1, \phi^-_1, \phi'^-_1, \phi''^-_1) \rangle = (v, 0, 0, 0) \sim (1, 4, -3/4)\,, \\ \langle \Phi^T_2 \rangle &= \langle (\phi^+_2, \phi^0_2, \phi'^0_2, \phi''^0_2) \rangle = (0, v', 0, 0) \sim (1, 4, 1/4)\,, \\ \langle \Phi^T_3 \rangle &= \langle (\phi^+_3, \phi^0_3, \phi'^0_3, \phi''^0_3) \rangle = (0, 0, V, 0) \sim (1, 4, 1/4)\,, \\ \langle \Phi^T_4 \rangle &= \langle (\phi^+_4, \phi^0_4, \phi'^0_4, \phi''^0_4) \rangle = (0, 0, 0, V') \sim (1, 4, 1/4)\,. \end{aligned} \tag{3.3}$$

[1]The three-family models for the parameter assignments $b = -1$, $c = -1$ $(b = -1,\ c = 2)$ are equivalent by hypercharge transformation to the models obtained for $b = 1$, $c = 1$ $(b = 1,\ c = -2)$.

Table 3.2.: Particle content for models E and F, the $\alpha = \{1, 2, 3\}$ are the lepton generation indices, i run over the first two generations of quarks. The numbers in parentheses refer to the $(SU(3)_C, SU(4)_L, U(1)_X)$ quantum numbers respectively.

Model E	Model F
$L_{L\alpha} = (\ e^-,\ \ \nu^0,\ \ N^0,\ \ E^-\ )_{L\alpha} \sim (1, \overline{4}, -1/2)$,	$L_{L\alpha} = (\ \nu^0,\ \ e^-,\ \ E^-,\ \ N^0\ )_{L\alpha} \sim (1, 4, -1/2)$,
$e^+_{L\alpha} \sim (1, 1, 1)$, $E^+_{L\alpha} \sim (1, 1, 1)$,	$e^+_{L\alpha} \sim (1, 1, 1)$, $E^+_{L\alpha} \sim (1, 1, 1)$,
$Q_{iL} = (\ u_i,\ \ d_i,\ \ D_i,\ \ U_i\ ) \sim (3, 4, 1/6)$,	$Q_{iL} = (\ d_i,\ \ u_i,\ \ U_i,\ \ D_i\ ) \sim (3, \overline{4}, 1/6)$,
$u^c_{iL} \sim (\overline{3}, 1, -2/3), d^c_{iL} \sim (\overline{3}, 1, 1/3)$,	$u^c_{iL} \sim (\overline{3}, 1, -2/3), d^c_{iL} \sim (\overline{3}, 1, 1/3)$,
$U^c_{iL} \sim (\overline{3}, 1, -2/3), D^c_{iL} \sim (\overline{3}, 1, 1/3)$,	$U^c_{iL} \sim (\overline{3}, 1, -2/3), D^c_{iL} \sim (\overline{3}, 1, 1/3)$,
$Q_{3L} = (\ d_3,\ \ u_3,\ \ U_3,\ \ D_3\ ) \sim (3, \overline{4}, -1/12)$,	$Q_{3L} = (\ u_3,\ \ d_3,\ \ D_3,\ \ U_3\ ) \sim (3, 4, 1/6)$,
$u^c_{3L} \sim (\overline{3}, 1, -2/3), d^c_{3L} \sim (\overline{3}, 1, 1/3)$,	$u^c_{3L} \sim (\overline{3}, 1, -2/3), d^c_{3L} \sim (\overline{3}, 1, 1/3)$,
$U^c_{3L} \sim (\overline{3}, 1, -2/3), D^c_{3L} \sim (\overline{3}, 1, 1/3)$,	$D^c_{3L} \sim (\overline{3}, 1, 1/3), U^c_{3L} \sim (\overline{3}, 1, -2/3)$,

The Model E and Model F are displayed in table 3.2. The scalar sector for this set of models is given by:

$$\begin{aligned}
\langle \Phi_1^T \rangle &= \langle (\phi_1^0, \phi_1^+, \phi_1'^+, \phi_1'^0) \rangle = (v, 0, 0, 0) \sim (1, \overline{4}, 1/2)\,, \\
\langle \Phi_2^T \rangle &= \langle (\phi_2^-, \phi_2^0, \phi_2'^0, \phi_2'^-) \rangle = (0, v', 0, 0) \sim (1, \overline{4}, -1/2)\,, \\
\langle \Phi_3^T \rangle &= \langle (\phi_3^-, \phi_3^0, \phi_3'^0, \phi_3'^-) \rangle = (0, 0, V, 0) \sim (1, \overline{4}, -1/2)\,, \\
\langle \Phi_4^T \rangle &= \langle (\phi_4^0, \phi_4^+, \phi_4'^+, \phi_4'^0) \rangle = (0, 0, 0, V') \sim (1, \overline{4}, 1/2)\,.
\end{aligned} \tag{3.4}$$

The pattern of the electroweak symmetry breaking (EWSB) goes as follows

$$SU(4)_L \otimes U(1)_X \xrightarrow{V'} SU(3)_L \otimes U(1)_{X'} \xrightarrow{V} SU(2)_L \otimes U(1)_Y \xrightarrow{v,v'} U(1)_{\rm Q}, \tag{3.5}$$

where $V' \sim V \gg v' \sim v$, and $v'^2 + v^2 = v^2_{\rm SM} \equiv (246\ {\rm GeV})^2$.

3.2. Dimension 5 effective operator

Neutrinos may acquire masses after the introduction of non-renormalizable[2] dimension-five operators defined as:

$$\mathcal{L}_5 = \frac{\mathcal{O}_5}{\Lambda}, \quad \mathcal{O}_5 = \{\overline{L^c_{L\alpha}} \Phi_i^\star \Phi_j^\dagger L_{L\beta}, \overline{L^c_{L\alpha}} \Phi_i \Phi_j^{\star\dagger} L_{L\beta}\}, \tag{3.6}$$

[2]Operators of energy dimension greater than four in the lagrangian of the theory.

being α and β lepton generation indices and i, j index in the number of scalar 4-plets. In Eq. (3.6), Λ represent the cutoff scale where new physics is expected. The operator given in Eq. (3.6) is the generalization of the Weinberg operator [8] for $SU(4)_L \otimes U(1)_X$. Depending on the way as the fields transforms under $SU(4)_L \otimes U(1)_X$, different tree-level realizations of the operator are allowed.

Table 3.3.: Scenarios for the operator defined in Eq. (3.6): In the left part, the $(4(\overline{4}), X_{L(\Phi)})$ notation represents the way as the fields (either $L_{L\alpha}$ or Φ_i) transforms under $SU(4)_L \otimes U(1)_X$. The effective operator is allowed if it is gauge invariant.

$L_{L\alpha}$	Φ_k	$\mathcal{O}_5^I = \overline{L^c_{L\alpha}}\Phi_i^\star\Phi_j^\dagger L_{L\beta}$	$\mathcal{O}_5^{II} = \overline{L^c_{L\alpha}}\Phi_i\Phi_j^{\star\dagger} L_{L\beta}$
$(4, X_L)$	$(4, X_\Phi)$	$4\otimes\overline{4}\otimes\overline{4}\otimes 4 \supset 1,\ \ 2X_L - 2X_\Phi = 0$	$4\otimes 4\otimes 4\otimes 4 \supset 1,\ \ 2X_L + 2X_\Phi = 0$
$(4, X_L)$	$(\overline{4}, X_\Phi)$	$4\otimes 4\otimes 4\otimes 4 \supset 1,\ \ 2X_L - 2X_\Phi = 0$	$4\otimes\overline{4}\otimes\overline{4}\otimes 4 \supset 1,\ \ 2X_L + 2X_\Phi = 0$
$(\overline{4}, X_L)$	$(4, X_\Phi)$	$\overline{4}\otimes\overline{4}\otimes\overline{4}\otimes\overline{4} \supset 1,\ \ 2X_L - 2X_\Phi = 0$	$\overline{4}\otimes 4\otimes 4\otimes\overline{4} \supset 1,\ \ 2X_L + 2X_\Phi = 0$
$(\overline{4}, X_L)$	$(\overline{4}, X_\Phi)$	$\overline{4}\otimes 4\otimes 4\otimes\overline{4} \supset 1,\ \ 2X_L - 2X_\Phi = 0$	$\overline{4}\otimes\overline{4}\otimes\overline{4}\otimes\overline{4} \supset 1,\ \ 2X_L + 2X_\Phi = 0$

For any set of fields (Φ, L_L), transforming in a general way under $SU(4)_L \otimes U(1)_X$, different theoretical realizations of the operators are displayed in table 3.3. In order to allow such an operators into an effective lagrangian, we must garanteed that the product of the irreducible representations contain the $SU(4)$ singlet and be hyperchargeless. Since for $SU(N)$, $N \otimes N = [(N^2+N)/2]_{\rm S} + [(N^2-N)/2]_{\rm A}$ and $N \otimes N^\star = [N^2-1]_{\rm Adjoint} + [1]$, there are only two possible main topologies for the tree-level realization of the Weinberg operator. From Eq. (3.6), if the intermediate particle is a scalar, it can transform as $10_{\rm S}$ and $15_{\rm Adjoint}$[3] under $SU(4)_L$, on the other hand if it is a fermion, it can transform as 1_A, and $15_{\rm Adjoint}$ under $SU(4)_L$[4]. In Figure 3.1 are displayed all the possible tree level realization of the effective Weinberg operator in the $SU(4)_L \otimes U(1)_X$ electroweak extension. The theory reduces to a canonical seesaw, a type II-like seesaw, and a type III-like seesaw in where, for $SU(4)_L$ a -fermion singlet, scalar decuplet and fermion 15-plet - are included respectively.

To our knowledge the 3-4-1 extension with a fermion singlet (canonical seesaw mechanism) has been implemented [74], as well as with a scalar decuplet [26, 75], but the fermion 15-plet has not been proposed in the literature yet. Those new particles in case of be added should have hypercharge values that does not spoil the anomaly free structure

[3] The scalar singlet does not gives rise to neutrino masses.

[4] The fermion sextet is also a possible realization of the Weinger operator, however is not allowed because after their introduction it does not give rise to neutrino masses, instead is an additional term that contribute to the masses of the charges leptons.

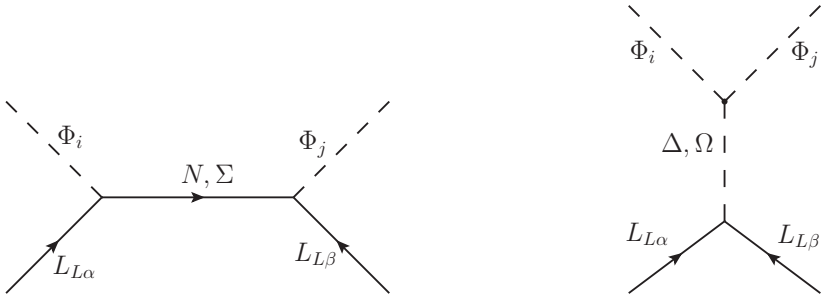

Figure 3.1.: Topologies of the Weinberg-like effective operator. On the left hand side the intermediate particle could be an $SU(4)$ fermion singlet $N_R \sim (1,0)$, and a fermion 15-plet $\Sigma \sim (15,0)$. On the right hand side the intermediate particles could be an $SU(4)$ scalar decuplet $\Delta \sim (10, X_\Delta)$ and a scalar 15-plet $\Omega \sim (15, X_\Omega)$.

of the model. That is why any new fermion content should have zero hypercharge or be a vector-like particle under $SU(4)_L$. In the next subsections, we display the set of effective Weinberg-like operators that can be built in the four models presented in section 3.1.

3.2.1. Model A

In this model there are a total of 9 operators, which are given by:

$$\begin{aligned}\mathcal{O}_5 \;=\; \Big\{ & \overline{L^c_{L\alpha}}\Phi_2\Phi_2^{\star\dagger}L_{L\beta},\;\; \overline{L^c_{L\alpha}}\Phi_2\Phi_3^{\star\dagger}L_{L\beta},\;\; \overline{L^c_{L\alpha}}\Phi_3\Phi_2^{\star\dagger}L_{L\beta}, \\ & \overline{L^c_{L\alpha}}\Phi_2\Phi_4^{\star\dagger}L_{L\beta},\;\; \overline{L^c_{L\alpha}}\Phi_4\Phi_2^{\star\dagger}L_{L\beta},\;\; \overline{L^c_{L\alpha}}\Phi_3\Phi_3^{\star\dagger}L_{L\beta}, \\ & \overline{L^c_{L\alpha}}\Phi_3\Phi_4^{\star\dagger}L_{L\beta},\;\; \overline{L^c_{L\alpha}}\Phi_4\Phi_3^{\star\dagger}L_{L\beta},\;\; \overline{L^c_{L\alpha}}\Phi_4\Phi_4^{\star\dagger}L_{L\beta} \Big\}\,. \end{aligned} \tag{3.7}$$

For this model we have:

1. $\Phi_k\Phi_k^{\star\dagger} \Rightarrow 4 \otimes 4 = 6_{\rm A} \oplus 10_{\rm S}$, therefore a $10_{\rm S}$ scalar is allowed as the intermediate particle. The $6_{\rm A}$ is not allowed because of its statistic.

2. $\Phi_k^{\star\dagger}L_{L\beta} \Rightarrow 4 \otimes \overline{4} = 1 \oplus 15_{\rm Adjoint}$, then either a fermion singlet or a fermion 15-plet are allowed as intermediate particles.

The operators defined in Eq. (3.7) have two topologies at the tree-level, one in which the intermediate particle is a fermion, either singlet $N_R \sim (1,1,0)$ or 15-plet $\Sigma \sim (1,15,0)$, and the other one in which the intermediate particle is a scalar decuplet $\Delta \sim (1,10,1/2)$. In order to fit all the experimental neutrino oscillation parameters, at least three right-handed neutrinos (three fermion 15-plet) per lepton generation or an scalar decuplet must be added.

3.2.2. Model B

For this model the operator is unique and is given by:

$$\mathcal{O}_5 = \left\{ \overline{L^c_{L\alpha}} \Phi_1^\star \Phi_1^\dagger L_{L\beta} \right\} . \tag{3.8}$$

1. $\Phi_k^\star \Phi_k^\dagger \Rightarrow \overline{4} \otimes \overline{4} = 6_{\rm A} \oplus \overline{10_{\rm S}}$, therefore a $\overline{10_{\rm S}}$ scalar is allowed as the intermediate particle, the 6_A is forbidden due to its statistic.

2. $\Phi_k^\dagger L_{L\beta} \Rightarrow \overline{4} \otimes 4 = 1 \oplus 15_{\rm Adjoint}$, then either a fermion singlet or a fermion 15-plet are allowed as intermediate particles.

The operators given in Eq. (3.8) has two topologies at tree level, one in which the intermediate particle is a fermion, either singlet $N_R \sim (1,1,0)$ or 15-plet $\Sigma \sim (1,15,0)$, and the other one in which the intermediate particle is a scalar decuplet $\Delta \sim (1,10,3/2)$. Again, to fit all the experimental neutrino oscillation parameters, at least one right-handed neutrino (15-plet fermion) per lepton generation or an scalar decuplet must be included.

3.2.3. Model E

For this model there are 4 operators, which are given by:

$$\mathcal{O}_5 \;=\; \left\{ \overline{L^c_{L\alpha}} \Phi_2^\star \Phi_2^\dagger L_{L\beta},\;\; \overline{L^c_{L\alpha}} \Phi_2^\star \Phi_3^\dagger L_{L\beta},\;\; \overline{L^c_{L\alpha}} \Phi_3^\star \Phi_2^\dagger L_{L\beta},\;\; \overline{L^c_{L\alpha}} \Phi_3^\star \Phi_3^\dagger L_{L\beta} \right\} . \tag{3.9}$$

1. $\Phi_k^\star \Phi_k^\dagger \Rightarrow 4 \otimes 4 = 6_{\rm A} \oplus 10_{\rm S}$, then a $10_{\rm S}$ scalar is allowed as the intermediate particle, the 6_A is not allowed because its statistic.

2. $\Phi_k^\dagger L_{L\beta} \Rightarrow 4 \otimes \overline{4} = 1 \oplus 15_{\rm Adjoint}$, then either a fermion singlet or a fermion 15-plet are allowed as intermediate particles.

Again, each of the previous operators have two topologies at tree level, one in which the intermediate particle is a fermion either singlet $N_R \sim (1,1,0)$ or 15-plet $\Sigma \sim (1,15,0)$, and the other one in which the intermediate particle is a scalar decuplet $\Delta \sim (1,10,1)$. In order to fit all the experimental neutrino oscillation parameters, at least two right-handed neutrinos (two fermion 15-plet) per lepton generation or an scalar decuplet must be added.

3.2.4. Model F

For this model there are 4 operators, which are given by:

$$\mathcal{O}_5 \;=\; \left\{ \overline{L^c_{L\alpha}} \Phi_1 \Phi_1^{\star\dagger} L_{L\beta},\;\; \overline{L^c_{L\alpha}} \Phi_1 \Phi_4^{\star\dagger} L_{L\beta},\;\; \overline{L^c_{L\alpha}} \Phi_4 \Phi_1^{\star\dagger} L_{L\beta},\;\; \overline{L^c_{L\alpha}} \Phi_4 \Phi_4^{\star\dagger} L_{L\beta} \right\} . \quad (3.10)$$

1. $\Phi_k \Phi_k^{\star\dagger} \Rightarrow \overline{4} \otimes \overline{4} = 6_{\rm A} \oplus \overline{10_{\rm S}}$, then a $\overline{10_{\rm S}}$ scalar is allowed as the intermediate particle, the $6_{\rm A}$ is not allowed because of its statistic.

2. $\Phi_k^{\star\dagger} L_{L\beta} \Rightarrow \overline{4} \otimes 4 = 1 \oplus 15_{\rm Adjoint}$, then either a fermion singlet or a fermion 15-plet are allowed as intermediate particles.

The operators given in Eq. (3.10) have two topologies at tree level, one in which the intermediate particle is a fermion either singlet $N_R \sim (1,1,0)$ or 15-plet $\Sigma \sim (1,15,0)$, and the other one in which the intermediate particle is a scalar decuplet $\Delta \sim (1,10,1)$. Neutrino oscillation parameters are explained after the model is extended with two right-handed neutrinos (or two fermion 15-plets) per lepton generation or a scalar decuplet.

To address neutrino masses and mixing, models with fermion singlets [74, 76] as well as with scalar decuplets have been constructed [75]. In particular, in Ref. [77] not new particles were introduced, instead the 10_S scalar representation was built using the fundamental representation of the scalar fields content in $SU(4)_L$. Scalar decuplets also have been used to provide masses for the charged leptons in 3-4-1 models [78]. In the next section we study the neutrino mass generation and mixing in the model F, extending with a fermion singlets, and a scalar decuplet.

3.3. Neutrino masses in Model F

In order to explain neutrino masses and mixing in the 3-4-1 electroweak extension, we explore the tree-level realization of the Weinberg-like operator in the model F introduced[5] in table 3.2.

[5]The same can be done for all the models, following the general classification given in chapter 3.2.

3.3.1. Canonical Seesaw Mechanism

The model F is extended with two right-handed neutrinos $N_{1\mathrm{R}i} \sim (1,1,0)$ and $N_{2\mathrm{R}i} \sim (1,1,0)$, being i the generation index. At least three generations of $\{N_{1\mathrm{R}i}, N_{2\mathrm{R}i}\}$ are needed in order explain the neutrino masses. The most general Yukawa lagrangian for the neutral lepton sector, including the new fields reads:

$$\begin{aligned} -\mathcal{L}_{\mathrm{yuk}} &= \Big[\lambda_1^{\alpha i}\overline{L_{L\alpha}}\Phi_1 N_{1Ri} + \lambda_2^{\alpha j}\overline{L_{L\alpha}}\Phi_1 N_{2Rj} + \lambda_3^{\alpha i}\overline{L_{L\alpha}}\Phi_4 N_{1Ri} \\ &+ \lambda_4^{\alpha j}\overline{L_{L\alpha}}\Phi_4 N_{2Rj} + h.c\Big] + \frac{1}{2}M_1\overline{N_{1Ri}^C}N_{1Ri} + \frac{1}{2}M_2\overline{N_{2Rj}^C}N_{2Rj} \\ &+ \left[\mu\overline{N_{1Ri}^C}N_{2Rj} + h.c\right], \end{aligned} \tag{3.11}$$

where $\lambda_l^{\alpha i}$; for $l \in \{1,2,3,4\}$ and $i \in \{1,2\}$, are $3\times k$ Yukawa matrix entries; k, the number of right-handed neutrinos per lepton generation, M_1 and M_2 are 3×3 Majorana mass matrices for the right-handed neutrinos and are assumed to be diagonal without loss of generality. The mixing term μ, is in general, allowed by the gauge symmetry. After the electroweak symmetry breaking (EWSB), Eq. (3.11) becomes:

$$-\mathcal{L}_{\mathrm{yuk}} = \begin{pmatrix}\overline{\nu_{L\alpha}} & \overline{N_{L\alpha}} & \overline{N_{1Ri}^C} & \overline{N_{2Ri}^C}\end{pmatrix}\mathcal{M}\begin{pmatrix}\nu_{L\alpha}\\ N_{L\alpha}\\ N_{1Ri}\\ N_{2Ri}\end{pmatrix}, \tag{3.12}$$

with:

$$\mathcal{M} = \begin{pmatrix} 0 & 0 & v\lambda_1 & v\lambda_2 \\ 0 & 0 & V'\lambda_3 & V'\lambda_4 \\ v\lambda_1^\dagger & V'\lambda_3^\dagger & M_1 & \mu \\ v\lambda_2^\dagger & V'\lambda_4^\dagger & \mu & M_2 \end{pmatrix} \equiv \begin{pmatrix} 0 & 0 & m_{1D} & m_{2D} \\ 0 & 0 & m_{3D} & m_{4D} \\ m_{1D}^\dagger & m_{3D}^\dagger & M_1 & \mu \\ m_{2D}^\dagger & m_{4D}^\dagger & \mu & M_2 \end{pmatrix} \equiv \begin{pmatrix} 0_{6\times 6} & M_D \\ M_D^\dagger & M_R \end{pmatrix} \tag{3.13}$$

The mass matrix given in Eq. (3.13) can not be diagonalized exactly. However for simplicity and illustrative purposes we set all element of matrix μ to be zero. In this model, the smallness of active neutrinos is due to the heavyness of the right-handed neutrinos as happens in the SM with the type I seesaw mechanism. In the limit $\{M_1, M_2\} >> \{m_{1D}, m_{2D}, m_{3D}, m_{4D}\}$, the mass matrix in Eq. (3.13) can be diagonalized

by blocks in an approximately way, and the masses for the lightest and heaviest neutrinos takes the form:

$$\mathcal{M}^{\text{light}} = -M_R^{-1} M_D M_D^{\dagger} + \mathcal{O}(M_R^{-2}) \approx - \begin{pmatrix} \alpha & \beta \\ \gamma & \delta \end{pmatrix} , \tag{3.14}$$

$$\mathcal{M}^{\text{heavy}} = M_R + \mathcal{O}(M_R^{-1}) \approx \begin{pmatrix} M_1 & 0 \\ 0 & M_2 \end{pmatrix} , \tag{3.15}$$

where

$$\begin{aligned} \alpha &= M_1^{-1}[m_{1D} m_{1D}^{\dagger} + m_{2D} m_{2D}^{\dagger}] , \\ \beta &= M_1^{-1}[m_{1D} m_{3D}^{\dagger} + m_{2D} m_{4D}^{\dagger}] , \\ \gamma &= M_2^{-1}[m_{3D} m_{1D}^{\dagger} + m_{4D} m_{2D}^{\dagger}] \equiv M_2^{-1} \beta^{\dagger} M_1 , \\ \delta &= M_2^{-1}[m_{3D} m_{3D}^{\dagger} + m_{4D} m_{4D}^{\dagger}] . \end{aligned} \tag{3.16}$$

From Eq. (3.14), the lightest neutrino spectrum in the physical basis is obtained as:

$$\mathcal{M}_{\text{diag}}^{\text{light}} = U^{\dagger} \mathcal{M}^{\text{light}} U , \tag{3.17}$$

being U a 6×6 matrix which mixed the lightest neutrinos [79]:

$$U^{6\times 6} = \begin{pmatrix} N^{3\times 3} & S^{3\times 3} \\ T^{3\times 3} & V^{3\times 3} \end{pmatrix} . \tag{3.18}$$

From the experimental side, oscillations between the three active SM neutrinos and exotic neutrinos have not yet being observed [80], implying that new neutral leptons, if they exist, must be heavy, $m_{N_L} > 1$ eV. As a consequence, the mixing matrices $S^{3\times 3}$ and $T^{3\times 3}$ in Eq. (3.18) will be suppressed. As pointed out [79], the current experimental limits on neutrinos oscillation experiments are not able to put stringent constraints in any of the new physics (NP) parameters given inside Eq. (3.18); however, a future generation of neutrino experiments will open the window for the exploration of neutrino oscillation parameters as well as CP-violation in the lepton sector [81]. The lepton flavor violation (LFV) processes such as $\mu \to e\gamma$ can take place in this model at one loop level, however a full study on LFV is beyond scope of this chapter. The lightest active SM neutrinos

acquire masses through the canonical seesaw mechanism, as happens for the SM. Based on the above observations, the mixing matrix in Eq. (3.18) is approximately diagonal[6], and the masses for the lightest SM neutrinos takes the form:

$$\begin{aligned} \mathcal{M}^{\rm diag}_{\widehat{\nu}_L} &\approx N^\dagger \mathcal{M}_{\nu_L} N \ , \\ \mathcal{M}^{\rm diag}_{\widehat{\nu}_L} &\approx U^\dagger_{\rm PMNS} M_1^{-1} [m_{1D} m_{1D}^\dagger] U_{\rm PMNS} \ , \end{aligned} \tag{3.19}$$

with $U_{\rm PMNS}$, the Pontecorvo-Maki-Nakagawa-Sakata mixing matrix [82] and $\mathcal{M}^{\rm diag}_{\widehat{\nu}_L} = {\rm diag}(m_{\nu 1}, m_{\nu 2}, m_{\nu 3})$. The masses for the lightest sterile neutrinos[7] reads,

$$\begin{aligned} \mathcal{M}^{\rm diag}_{\widehat{N}_L} &\approx V^\dagger \mathcal{M}_{N_L} V \ , \\ \mathcal{M}^{\rm diag}_{\widehat{N}_L} &\approx V^\dagger M_2^{-1} [m_{4D} m_{4D}^\dagger] V^\dagger \ , \end{aligned} \tag{3.20}$$

with $\mathcal{M}^{\rm diag}_{\widehat{N}_L} = {\rm diag}(m_{N1}, m_{N2}, m_{N3})$. The Eq. (3.19) and Eq. (3.20) were obtained after demanding $\lambda_1 \gg \lambda_2$ and $\lambda_4 \gg \lambda_3$. Under these assumptions the two neutrino sectors are uncorrelated. The masses for the SM neutrinos are fully determined by M_1, λ_1 and $U_{\rm PMNS}$.

3.3.2. Type II-like Seesaw Mechanism

The model F displayed in table 3.2 is extended with a scalar decuplet $\Delta \sim (1, 10, 1)$. The most general lagrangian for the neutral leptons is given by:

$$-\mathcal{L}_{\rm yuk} = y_{\alpha\beta} \overline{\widetilde{L^C_{L\alpha}}} \Delta L_{L\beta} + h.c. \ , \tag{3.21}$$

where, $y_{\alpha\beta}$ is a symmetric mixing matrix, $\overline{\widetilde{L^C_L}} = \overline{L^C_L} i\sigma \equiv (-\overline{e^C}, \overline{\nu^C}, -\overline{N^C}, \overline{E^C})$, being

$$\sigma = T_{2L} + T_{14L} = \frac{1}{2} \begin{pmatrix} 0 & -i & 0 & 0 \\ i & 0 & 0 & 0 \\ 0 & 0 & 0 & -i \\ 0 & 0 & i & 0 \end{pmatrix} . \tag{3.22}$$

[6] There are not mixing between the sterile neutrinos and the SM ones.
[7] Neutral lepton with no ordinary weak interactions except those induced by mixing.

The scalar decuplet contains ten degrees of freedom, using a canonical kinetic term; those can be parametrized as:

$$\Delta = \begin{pmatrix} \Delta_{11}^{+} & \Delta_{12}^{++} & \Delta_{13}^{++} & \Delta_{14}^{+} \\ \Delta_{21}^{0} & \Delta_{22}^{+} & \Delta_{23}^{+} & \Delta_{24}^{0} \\ \Delta_{31}^{0} & \Delta_{32}^{+} & \Delta_{33}^{+} & \Delta_{34}^{0} \\ \Delta_{41}^{+} & \Delta_{42}^{++} & \Delta_{43}^{++} & \Delta_{44}^{+} \end{pmatrix} \equiv \begin{pmatrix} \frac{1}{\sqrt{2}}H_1^{+} & H_1^{++} & \frac{1}{\sqrt{2}}H_2^{++} & \frac{1}{\sqrt{2}}H_3^{+} \\ H_1^{0} & -\frac{1}{\sqrt{2}}H_1^{+} & -\frac{1}{\sqrt{2}}H_2^{+} & \frac{1}{\sqrt{2}}H_3^{0} \\ -\frac{1}{\sqrt{2}}H_3^{0} & \frac{1}{\sqrt{2}}H_3^{+} & -\frac{1}{\sqrt{2}}\omega^{+} & -\kappa^{0} \\ \frac{1}{\sqrt{2}}H_2^{+} & -\frac{1}{\sqrt{2}}H_2^{++} & \rho^{++} & \frac{1}{\sqrt{2}}\omega^{+} \end{pmatrix} . \quad (3.23)$$

After EWSB, the neutral components of the decuplet develop a VEV and the lagrangian in Eq. (3.21) becomes:

$$\begin{aligned} -\mathcal{L}_{\text{yuk}} &= y_{\alpha\beta}\Big(\overline{\nu_{L\alpha}^{c}}\langle H_1^0\rangle\ \nu_{L\beta} + \frac{1}{\sqrt{2}}\overline{\nu_{L\alpha}^{c}}\langle H_3^0\rangle N_{L\beta} \\ &+ \frac{1}{\sqrt{2}}\overline{N_{L\alpha}^{c}}\langle H_3^0\rangle\nu_{L\beta} + \overline{N_{L\alpha}^{c}}\langle\kappa^0\rangle N_{L\beta}\Big) + h.c \\ &= \begin{pmatrix}\overline{\nu_{L\alpha}^{c}} & \overline{N_{L\alpha}^{c}}\end{pmatrix}\mathcal{M}\begin{pmatrix}\nu_{L\beta} \\ N_{L\beta}\end{pmatrix} , \end{aligned} \quad (3.24)$$

with

$$\mathcal{M} = \begin{pmatrix} y_{\alpha\beta}\langle H_1^0\rangle & \frac{1}{\sqrt{2}}y_{\alpha\beta}\langle H_3^0\rangle \\ \frac{1}{\sqrt{2}}y_{\alpha\beta}\langle H_3^0\rangle & y_{\alpha\beta}\langle\kappa^0\rangle \end{pmatrix} , \quad (3.25)$$

with α and β being lepton generation indices. We demand $\langle H_3^0\rangle < 1$ GeV, in order to avoid $e-E$ large mixing. The scalar decuplet will modified the tree-level ρ parameter [38].

$$\rho^{\text{tree}} \simeq 1 - \frac{2\langle H_1^0\rangle^2}{v^2 + v'^2 + \langle H_1^0\rangle^2} . \quad (3.26)$$

Since, $\rho_{\text{exp}} = 1.00040 \pm 0.00024$ [65], in order to satisfy the ρ constraint, $\langle H_1^0\rangle \leq 1.5$ GeV. Notice that $\langle\kappa^0\rangle$ is not constrained by ρ. Assuming $\{\langle H_1^0\rangle, \langle H_3^0\rangle\} < \langle\kappa^0\rangle$, the neutrino masses for the lightest SM neutrinos and the heavy ones at second order in perturbative diagonalization takes the form:

$$\mathcal{M}_{\text{Light}} = y_{\alpha\beta}\langle H_1^0\rangle - \frac{\langle H_3^0\rangle^2}{\langle\kappa^0\rangle}y_{\alpha\beta}^{-1}y_{\alpha\beta}y_{\alpha\beta}^{\dagger} , \quad (3.27)$$

$$\mathcal{M}_{\text{Heavy}} = y_{\alpha\beta}\langle\kappa^0\rangle + \frac{\langle H_3^0\rangle^2}{\langle\kappa^0\rangle}y_{\alpha\beta}^{-1}y_{\alpha\beta}y_{\alpha\beta}^{\dagger} . \quad (3.28)$$

In the limit $\langle H_3^0 \rangle \ll \langle \kappa^0 \rangle$, the Eq. (3.27) and Eq. (3.28) are diagonalized by the same $U_{\rm PMNS}$ mixing matrix [8].

$$\mathcal{M}_{\nu}^{\rm diag} = U_{PMNS}^{\dagger}\mathcal{M}_{\rm Light}U_{PMNS} = \langle H_1^0 \rangle\, U_{PMNS}^{\dagger}\, \mathbf{Y}\, U_{PMNS}\ , \tag{3.29}$$

$$\mathcal{M}_{\rm N}^{\rm diag} = U_{PMNS}^{\dagger}\mathcal{M}_{\rm Heavy}U_{PMNS} = \langle \kappa^0 \rangle\, U_{PMNS}^{\dagger}\, \mathbf{Y}\, U_{PMNS}\ , \tag{3.30}$$

where leptonic indices has been suppressed in matrix $\mathbf{Y}$. Since both matrices; $\mathcal{M}_{\rm Heavy}$ and $\mathcal{M}_{\rm Light}$ are diagonalized by the same matrix, then the heavy neutral leptons (exotics) and the lightest (SM ones) has the same mass hierarchy. Therefore,

$$\begin{aligned} \mathcal{M}_{\rm Ni}^{\rm diag} &= \frac{\langle \kappa^0 \rangle}{\langle H_1^0 \rangle}\mathcal{M}_{\nu i}^{\rm diag}\ , \\ \begin{pmatrix} m_{N1} & 0 & 0 \\ 0 & m_{N2} & 0 \\ 0 & 0 & m_{N3} \end{pmatrix} &= \frac{\langle \kappa^0 \rangle}{\langle H_1^0 \rangle} \begin{pmatrix} m_{\nu 1} & 0 & 0 \\ 0 & m_{\nu 2} & 0 \\ 0 & 0 & m_{\nu 3} \end{pmatrix}\ . \end{aligned} \tag{3.31}$$

Using the data from neutrino oscillation [80], the lightest of the sterile neutrino satisfies $M_{N1} > 1$ eV. From this we derived the next constraints on the VEV of the scalar decuplet.

$$\langle \kappa^0 \rangle > \frac{1\ \text{eV}\langle H_1^0 \rangle}{m_{\nu 1}} \tag{3.32}$$

Assuming for instance $m_{\nu 1} \simeq \sqrt{\Delta m_{12}^2} \simeq 8.717 \times 10^{-3}$ eV, which is the maximum possible value for $m_{\nu 1}$ in the normal hierarchy (NH) scenario[55], then $\langle \kappa^0 \rangle > \ 114.707\ \langle H_1^0 \rangle$, is a lower bound on $\langle \kappa^0 \rangle$ derived from neutrino physics. In this model, LFV processes such as $\mu^- \to e^+e^-e^-$, $\tau^- \to e^+e^-e^-$, $\tau^- \to \mu^+\mu^-\mu^-$ are mediated by H_1^{++} at the tree-level. These processes are controlled by $y_{\alpha\beta}$ and also depends of the new scalar sector spectrum.

$$\begin{aligned} \text{BR}(\mu^- \to e^+e^-e^-) &\approx \frac{\Gamma(\mu^- \to e^+e^-e^-)}{\Gamma(\mu^- \to e^+\nu_\mu\overline{\nu_e})}\ , \\ &= \frac{1}{(M_{H_1^{++}})^4 G_F^2}|y_{\mu e}|^2|y_{ee}|^2\ . \end{aligned} \tag{3.33}$$

$\text{BR}(\mu^- \to e^+e^-e^-)$ is constrained [83] to satisfy $\text{BR}(\mu^- \to e^+e^-e^-) < 1.0 \times 10^{-12}$, which is the most severe limit. In figure 3.2 is displayed the $\text{BR}(\mu^- \to e^+e^-e^-)$ as a function of y_{ee}. The vertical dashed line are the points with yukawa couplings of order $\sim 4\pi$, which

[8] The same conclusion is draw for Eq. (3.27) and Eq. (3.28) forcing $y_{\alpha\beta}$ to be real, assumption which is not general, and only will be valid for a real $U_{\rm PMNS}$.

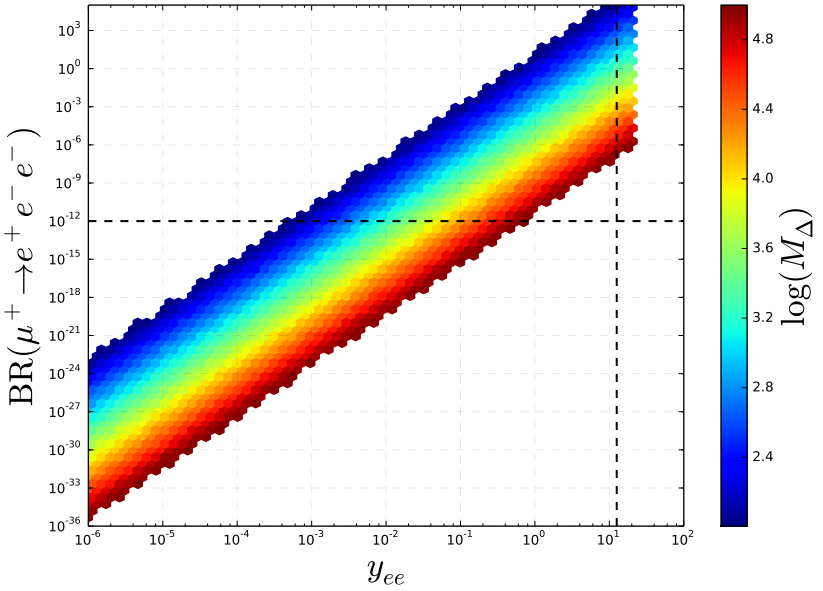

Figure 3.2.: $\mathrm{BR}(\mu^- \to e^+ e^- e^-)$ as a function of y_{ee}. The vertical dashed line represent the point where couplings of order $\sim 4\pi$ are expected, and the horizontal dashed line is the upper limit for $\mathrm{BR}(\mu^- \to e^+ e^- e^-)$ process.

represents the perturbative limit. To the left of that line neutrino masses and mixing are explained. The points with $y_{ee} > 4\pi$ are ruled out by perturbativity. The horizontal dashed line represents the upper limit on $\mathrm{BR}(\mu^- \to e^+ e^- e^-)$, above that limit the points are ruled out. All the points in the plot were obtained performing a scan of the following parameters in the range

$$\begin{aligned} 100\ \text{GeV} < \quad & m_{H_1^{++}} & < 100\ \text{TeV}\ , \\ 10^{-9}\ \text{GeV} < \quad & \langle H_1^0 \rangle & < 1.5\ \text{GeV}\ , \\ 10^{-9}\ \text{GeV} < \quad & \langle H_3^0 \rangle & < 1\ \text{GeV}\ , \\ 10^{-7} < \quad & y_{\alpha\beta} & < 2 \times 10^1\ . \end{aligned}$$

All the points in figure 3.2 satisfy the neutrino mixing and masses constraints [55] at 2σ[9]. On the other hand, notice that model F account for neutrino masses and mixing extending it with two fermion 15−plet per lepton generation. Since the fermion 15-plet mixes with the charged 4-plet leptons, then tree-level LFV processes mediated by the neutral gauge bosons (Z, Z' and Z'') are present. The model will also have restrictions coming from colliders constraints on heavy exotic leptons. This model is very interesting,

[9] We only consider the case for the NH scenario.

its phenomenology is more richer than the two other realizations shown before, but is beyond scope this work and will be considered in a future work.

Chapter 4.

Radiative Type III seesaw and its colliders phenomenology

In this chapter we carry out a collider analysis in the Radiative seesaw model (RSIII), a scotogenic model in where an $SU(2)$ scalar doublet and a fermion triplet, both colorless, and transforming non-trivially under an exact Z_2 discrete symmetry are added to the standard model (SM). This model provides a natural Dark Matter (DM) candidate for the Universe and also account for the neutrino masses and mixing. Since the fermion triplets have gauge interactions, they may be copiously produced at the LHC. Exclusion as a function of the flavor is obtained for the RSIII for regions in the parameter space that agrees with dark matter relic density constraint and neutrino oscillation.

4.1. The model

In this section we introduce the model RSIII [44–46], an extension of the SM with an additional complex scalar doublet of $SU(2)$, Φ, and $n_\Sigma \geq 2$ generations of vector fermion triplets of $SU(2)$, Σ_k, $k = 1, \ldots, n_\Sigma$. The quantum numbers of the scalar and leptonic sector of the model are given in table 4.1. The new particles are odd under an exact $\mathbf{Z}_2$ discrete symmetry, forcing the lightest $\mathbf{Z}_2$-odd particle to be stable, and thus a natural DM candidate. This symmetry also prevents neutrino masses from being generated by the tree-level Type-III seesaw mechanism [15]. Neutrino masses are generated at the one-loop level [70] via their interactions with the neutral components of Σ_k, the Majorana

Table 4.1.: Gauge, $\mathbf{Z}_2$ and spin quantum numbers of the particle content of the RSIII entering $\mathcal{L}_{\rm NP}$, Eq. (4.2). Here α and k denote, respectively, the lepton flavor and NP fermion index.

	$SU(2)_L$	$U(1)_Y$	$\mathbf{Z}_2$	S
Φ_{SM}	2	1	+	0
Φ	2	1	−	0
L_α	2	−1	+	1/2
Σ_k	3	0	−	1/2

fermions Σ_k^0, and the neutral components of Φ, ϕ^0. Therefore, the $\mathbf{Z}_2$ symmetry plays a crucial role linking DM to the neutrino mass generation[1].

4.1.1. Lagrangian

The most general renormalizable Lagrangian of the RSIII reads

$$\mathcal{L}_{\rm RSIII} = \mathcal{L}_{\rm SM} + \mathcal{L}_{\rm NP} \ , \tag{4.1}$$

with [46]

$$\begin{aligned}\mathcal{L}_{\rm NP} = i{\rm Tr}\left[\overline{\Sigma}\not{D}\Sigma\right] - \frac{1}{2}{\rm Tr}\left[\overline{\Sigma}M_\Sigma\Sigma^c + \overline{\Sigma^c}M_\Sigma^*\Sigma\right] - \left(Y_{k\alpha}\widetilde{\Phi}^\dagger\overline{\Sigma_k}L_\alpha + {\rm h.}c.\right) \\ + (D_\mu\Phi)^\dagger(D^\mu\Phi) - V_{NP}(\Phi,\Phi_{SM})\,,\end{aligned} \tag{4.2}$$

with $\alpha = e,\mu,\tau$. Here the trace runs over the $SU(2)$ indices, the mass matrix M_Σ (but not the NP yukawa couplings Y) is assumed to be flavor diagonal, D denotes the covariant derivative, L are the left-handed lepton doublets, and Φ_{SM} is the SM scalar doublet. Whenever possible the flavor indices have been suppressed. The NP scalar

[1] It is worth mentioning that the evolution of the model parameters via the renormalization group equations may induce a non-zero vacuum expectation value for ϕ^0 at high scales, leading to the spontaneous breaking of the $\mathbf{Z}_2$ symmetry. This situation, that indeed occurs in the minimal scotogenic model [84], may be naturally avoided extending the model with a $\mathbf{Z}_2$-even real scalar-triplet, as shown in [85] in the context of the scotogenic model where a fermion singlet is replaced by a fermion triplet [86]. This solution, where the evolution of the couplings of the scalar sector is modified by the extension of the scalar sector, is fully applicable to our case.

potential is given by

$$V_{NP}(\Phi,\Phi_{SM}) = \mu_2^2\Phi^\dagger\Phi + \lambda_2(\Phi^\dagger\Phi)^2 + \lambda_3(\Phi_{SM}^\dagger\Phi_{SM})(\Phi^\dagger\Phi) + \lambda_4(\Phi_{SM}^\dagger\Phi)(\Phi^\dagger\Phi_{SM}) + \frac{\lambda_5}{2}\left[(\Phi_{SM}^\dagger\Phi)^2 + \text{h.}c.\right] , \tag{4.3}$$

with all the scalar couplings λ_i real.

The scalar fields are given by

$$\Phi = \begin{pmatrix} H^+ \\ \frac{1}{\sqrt{2}}(H^0 + iA^0) \end{pmatrix} , \qquad \Phi_{SM} = \begin{pmatrix} G^+ \\ \frac{1}{\sqrt{2}}(v + h + iG_I^0) \end{pmatrix} , \tag{4.4}$$

where G_I^0 and G^+ the Goldstone bosons of the SM, $\langle\Phi_{SM}\rangle = \begin{pmatrix} 0, & v/\sqrt{2} \end{pmatrix}^T$ with $v = 246$ GeV. The masses for the NP scalars can be obtained from Eq. (4.3):

$$\begin{aligned} m_{H^\pm}^2 &= \mu_2^2 + \frac{\lambda_3}{2}v^2 , \\ m_{H^0}^2 &= \mu_2^2 + \frac{(\lambda_3+\lambda_4+\lambda_5)}{2}v^2 , \\ m_{A^0}^2 &= \mu_2^2 + \frac{(\lambda_3+\lambda_4-\lambda_5)}{2}v^2 . \end{aligned} \tag{4.5}$$

where H^0 and A^0 denote the neutral scalar and pseudoscalar components of the $\mathbf{Z}_2$-odd scalar, and $H^\pm$ its charged components. The Higgs mass is fixed to its current experimental value measured by ATLAS and CMS, $m_h = 125.09 \pm 0.24$ GeV [87].

The mass ordered $\mathbf{Z}_2$-odd fermion fields, triplets of $SU(2)_L$, can be written as [46]

$$\Sigma_k = \begin{pmatrix} \Sigma_k^0/\sqrt{2} & \Sigma_k^+ \\ \Sigma_k^- & -\Sigma_k^0/\sqrt{2} \end{pmatrix} . \tag{4.6}$$

At tree level the masses for the neutral and charged $\mathbf{Z}_2$-odd fermion triplets Σ_k are degenerated within each generation. At one loop the mass splitting between the charged and neutral components of Σ_k can be computed with the general formula given in Ref. [88], resulting in a mass splitting of between $\Delta m_{\text{loop}} \approx 152$ MeV for small $m_{\Sigma_k^0}$, and $\Delta m_{\text{loop}}^{\max} = \alpha_2 M_W \sin^2(\theta_W/2) = 166 \pm 1$ MeV, its asymptotic value for large $m_{\Sigma_k^0}$. This mass difference is small enough to neglect decays of the charged fermion to the neutral one and a virtual W boson.

Since our analysis is not sensitive to the CP properties of the model we assume, without loss of generality, that the CP-even scalar H^0 is lighter than the CP-odd A^0. Therefore, H^0 is stable and the natural DM candidate. A convenient set of parameters to describe the full model are the masses of the unknown scalar spectrum $\{m_{H^0}, m_{A^0}, m_{H^\pm}\}$, the self-couplings λ_2, $\lambda_L \equiv \lambda_{H^0} = (\lambda_3 + \lambda_4 + \lambda_5)/2$, $n_\Sigma \times n_\Sigma$ complex yukawa couplings $Y_{k\alpha}$, and the n_Σ masses for the neutral components of the fermion triplet $m_{\Sigma_k^0}$.

4.1.2. Neutrino Mass Generation

In this model the neutrino masses arise at one-loop via their interaction with the $\mathbf{Z}_2$-odd fermions and scalars [45]. The corresponding Feynman diagram is displayed in Fig. 4.1. The neutrino mass matrix reads

$$
\begin{aligned}
(\mathcal{M}_\nu)_{\alpha\beta} &= \sum_{k=1}^{n_\Sigma} Y_{k\alpha} Y_{k\beta} \Lambda_k = \sum_{k=1}^{n_\Sigma} \left[Y^T \Lambda Y \right]_{\alpha\beta} \ , \qquad \alpha, \beta = 1, 2, 3 \ , \\
\Lambda_k &= \frac{m_{\Sigma_k^0}}{32\pi^2} \left[\frac{m_{H^0}^2}{m_{H^0}^2 - m_{\Sigma_k^0}^2} \ln\left(\frac{m_{H^0}^2}{m_{\Sigma_k^0}^2} \right) - \frac{m_{A^0}^2}{m_{A^0}^2 - m_{\Sigma_k^0}^2} \ln\left(\frac{m_{A^0}^2}{m_{\Sigma_k^0}^2} \right) \right] \ ,
\end{aligned}
\tag{4.7}
$$

where Λ_k are the entries of the diagonal matrix Λ. The special case $n_\Sigma = 2$ leads to a singular neutrino mass matrix with one vanishing eigenvalue. The physical neutrino masses are obtained diagonalising Eq.(4.7) with the Pontecorvo-Maki-Nakagawa-Sakata neutrino mixing matrix U_{PMNS} [82] (see Ref. [89] for its standard parametrization):

$$
U_{PMNS}^T \mathcal{M}_\nu U_{PMNS} = \mathrm{diag}(m_{\nu_e}, m_{\nu_\mu}, m_{\nu_\tau}) \equiv M_\nu^{diag} \ . \tag{4.8}
$$

Using the Casas-Ibarra parametrization procedure [90] we express the yukawa coupling matrix in terms of the new physics mass parameters included in Λ_k (4.7), and the experimental neutrino data:

$$
Y = \sqrt{\Lambda}^{-1} R \sqrt{M_\nu'^{diag}} U_{PMNS}^\dagger \ , \tag{4.9}
$$

where R is an arbitrary $n_\Sigma \times 3$ orthogonal matrix connecting $\mathbf{Z}_2$-odd fermion and lepton flavor space and $M_\nu'^{diag} = diag(m_{\nu_1}, m_{\nu_2}, m_{\nu_3})$. If $n_\Sigma > 2$ and the lightest neutrino is allowed to vary in its full experimentally allowed range both hierarchies cover almost

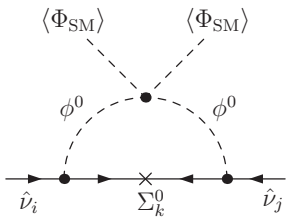

Figure 4.1.: One-loop neutrino mass generation in the RSIII via the exchange of a $\mathbf{Z}_2$-odd neutral scalar $\phi^0 = H^0, A^0$ and a $\mathbf{Z}_2$-odd fermion Σ_k^0. The neutrino interaction eigenstates are denote by $\hat{\nu_\alpha}$ and $\hat{\nu_\beta}$.

the whole range of normalized yukawa couplings, as can be observed in Fig. 4.2, where solutions of Eq. (4.9) with real R are shown in flavor space for the normal (NH) and inverse (IH) hierarchies. Here $\hat{Y}_\alpha \equiv \hat{Y}_{1\alpha} = Y_{1\alpha}/\sqrt{\sum_{\alpha=e,\mu,\tau}|Y_{1\alpha}|^2}$ denote the normalized yukawa couplings and the color shows the logarithmically averaged mass of lightest neutrino mass in each hierarchy. These solutions have been obtained for $\Sigma_k^\pm$ masses of $500, 1500$, and 2500 GeV. However, qualitatively similar solutions are obtained for different fermion masses. For our numerical analysis we will assume $n_\Sigma = 3$ and a normal hierarchy for the neutrino masses.

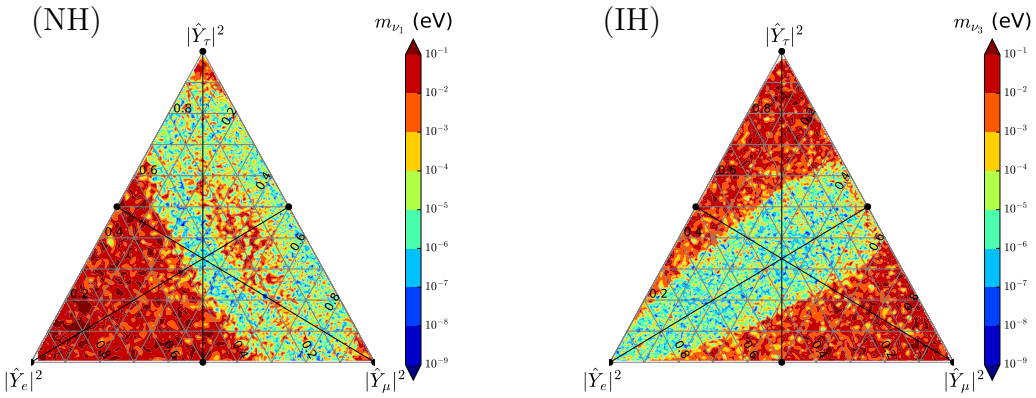

Figure 4.2.: Normal (NH) and inverse (IH) hierarchy solutions in flavor space (visualized as described in [91]). For every set of normalized yukawa couplings squared $|\hat{Y}_\alpha|^2, \alpha = e, \mu, \tau$, the lightest neutrino mass m_{ν_k} of the obtained solutions is averaged logarithmically.

4.1.3. Lepton Flavor Violation (LFV)

The LFV processes such as $\mu^- \to e^-\gamma$ vanish in the SM but arise in the RSIII at the one-loop via the LFV yukawa interactions with the $\mathbf{Z}_2$-odd scalars (4.2) shown in Fig. 4.3.

The analytic expression for $Br(\mu^- \to e^-\gamma)$ is given by

$$Br(\mu^- \to e^-\gamma) = \frac{3\alpha_{em} Br(\mu^- \to e^-\nu_\mu \overline{\nu}_e)}{256\pi^2 G_F^2} \times \left| \sum_{k=1}^{n_\Sigma} Y^*_{k\mu} Y_{ke} \left\{ \frac{1}{m^2_{H^\pm}} F_2\left(\frac{m^2_{\Sigma^0_k}}{m^2_{H^\pm}}\right) - \frac{1}{m^2_{\Sigma^\pm_k}} \left[F_2\left(\frac{m^2_{H^0}}{m^2_{\Sigma^\pm_k}}\right) + F_2\left(\frac{m^2_{A^0}}{m^2_{\Sigma^\pm_k}}\right) \right] \right\} \right|^2 , \tag{4.10}$$

with G_F the Fermi constant and

$$F_2(x) = \frac{1 - 6x + 3x^2 + 2x^3 - 6x^2 \log x}{6(x-1)^4} . \tag{4.11}$$

This expression can be trivially generalized to $\tau^- \to \mu^-\gamma$ and $\tau^- \to e^-\gamma$.

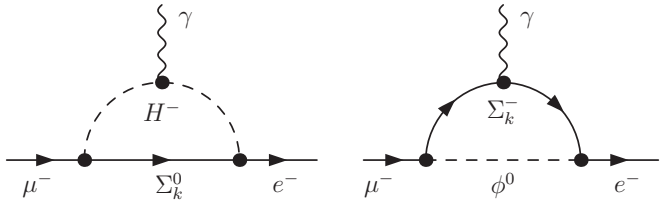

Figure 4.3.: Feynman diagrams contributing to $\mu^- \to e^-\gamma$. Here $\phi^0 = H^0, A^0$. Not shown are the self-energy corrections leading to electron-muon mixing.

4.1.4. Dark matter

The case of fermionic DM has been studied in [45, 46]. The DM candidate is the neutral component of the lightest NP fermion triplet. Since its electroweak couplings to gauge bosons are unsuppressed, the $\mathbf{Z}_2$-odd fermions need to be heavier than 2.6 TeV [46] in order to suppress the DM annihilation cross-section before freeze-out and thus allow for the correct relic density. Therefore, one does not expect significant phenomenological signatures at the LHC.

The scalar sector, on the other hand, allows for lighter DM. Since it has the same field content and couplings to the SM as the Inert Higgs Doublet Model [92], its phenomenology is also very similar. Scalar DM is viable both at around the electroweak scale, the "low mass region", as well as above 500 GeV [93]. We focus our analysis in the phenomenologically more interesting low mass region for DM. In this region the dominant

annihilation channels are $b\bar{b}$, mainly via the exchange of a Higgs boson in s-channel, and annihilation to gauge boson pairs for very small λ_L, or above the W^+W^- threshold.

4.2. Model Constraints

The RSIII model is constrained by direct and indirect searches for DM, colliders and electroweak precision observables. In this section we review the implication of these constraints on the parameter space of the model.

4.2.1. Theory constraints

The following conditions are obtained requiring that the scalar potential is bounded from below [94]: $\lambda_{1,2} > 0$, $\lambda_3 + \lambda_4 - |\lambda_5| + 2\sqrt{\lambda_1\lambda_2} > 0$ and $\lambda_3 + 2\sqrt{\lambda_1\lambda_2} > 0$. Requiring perturbativity sets bounds on the scalar couplings, $|\lambda_i| < 8\pi$, for $i = 1, \ldots, 5$. However, tree-level unitarity constraints [95, 96] set stronger bounds on these couplings (see Ref. [96]).

4.2.2. Electroweak precision observables

The contribution to the oblique parameters S, T, U from the $\mathbf{Z}_2$-odd scalar sector have been computed for the IDM in Refs. [97–99]. The contribution to S, T and U from the $\mathbf{Z}_2$-odd fermions, a triplet of $SU(2)_L$, vanish. As in the case of pure gauginos in the MSSM, they cannot contribute to operators with $SU(2)_L$-breaking quantum numbers, see e.g., [100–102]. The SM best fit obtained in [103] with a reference SM defined fixing $m_{t,ref} = 173$ GeV and $M_{H,ref} = 125$ GeV is

$$\begin{aligned} &\bar{S} = 0.05 \pm 0.11, \quad \bar{T} = 0.09 \pm 0.13, \quad \bar{U} = 0.01 \pm 0.11, \\ &\rho_{ST} = +0.90, \quad \rho_{SU} = -0.59, \quad \rho_{TU} = -0.83 \ , \end{aligned} \tag{4.12}$$

from which the correlation matrix is computed.

4.2.3. Collider constraints

LEP sets limits on the masses of all charged particles which can be directly produced, as well as on particles produced as their decay products. These limits can be easily

reinterpreted for the new scalars and fermions of the RSIII. The decays of gauge bosons into $\mathbf{Z}_2$-odd pairs are excluded by their invisible width measurements [89], leading to the constraints $m_{H^0,A^0} + m_{H^\pm} > M_W$, $m_{A^0} + m_{H^0} > M_Z$, $2m_{H^\pm} > M_Z$, $m_{\Sigma_1^0} + m_{\Sigma_1^\pm} > M_W$ and $2m_{\Sigma_1^\pm} > M_Z$. Since the $\mathbf{Z}_2$-odd fermions couple to gauge bosons with the same couplings as the gauginos we can apply the bounds on direct chargino searches at LEP II $m_{\Sigma_1^\pm} > 103.5$ GeV [60, 104–107]. Direct chargino searches at LEP II can also be reinterpreted for the search of charged scalars [108], leading to $m_{H^\pm} > 70$ GeV. The direct LEP search limits for associated scalar and gauge boson do not apply here due to the existence of the $\mathbf{Z}_2$ symmetry. We use the bounds obtained in [109]

$$\max(m_{A^0}, m_{H^0}) \gtrsim 100 \text{ GeV} \qquad \text{or} \qquad |m_{A^0} - m_{H^0}| < 8 \text{ GeV} \,. \tag{4.13}$$

The bound on the heavier neutral scalar varies between 100 GeV and 110 GeV as a function of the lightest scalar mass (see Fig. 7 of Ref. [109]). We require $\max(m_{A^0}, m_{H^0}) > 110$ GeV. The small allowed region for $\min(m_{A^0}, m_{H^0}) \geq m_W$ and $|m_{A^0} - m_{H^0}| > 8$ GeV which we exclude does not significantly affect our analysis.

The LHC sets bounds on the invisible and diphoton Higgs decays. If any of the channels $h \to H^0 H^0, A^0 A^0$, are open, they should satisfy the constraint on the upper limit for the invisible decay of the Higgs boson [110]

$$\sum_{\Phi^0 = H^0, A^0} \text{Br}(h \to \Phi^0 \Phi^0) < \text{Br}^{max}(h \to \text{inv.}) = 0.13 \,. \tag{4.14}$$

This upper limit is expected to be reduced by half at the future Run-II of the LHC [111]. For the diphoton channel, the signal strength $R_{\gamma\gamma}$ measures the ratio of the observed diphoton production cross section relative to the SM expectation [112]:

$$R_{\gamma\gamma} = \frac{\sigma(pp \to h \to \gamma\gamma)^{\text{RSIII}}}{\sigma(pp \to h \to \gamma\gamma)^{\text{SM}}} = \frac{\sigma(pp \to h \to \gamma\gamma)^{\text{IDM}}}{\sigma(pp \to h \to \gamma\gamma)^{\text{SM}}} \approx \frac{\left[\text{Br}(h \to \gamma\gamma)\right]^{\text{IDM}}}{\left[\text{Br}(h \to \gamma\gamma)\right]^{\text{SM}}} \,. \tag{4.15}$$

This relation holds since the $\mathbf{Z}_2$-odd fermions do not interact with the SM Higgs boson. The signal strength relative to the Standard Model expectation is measured by ATLAS [113] and CMS [114],

$$R_{\gamma\gamma}^{ATLAS} = 1.15 \pm {}^{+0.27}_{-0.25} \,, \qquad R_{\gamma\gamma}^{CMS} = 1.12 \pm {}^{+0.25}_{-0.23} \,. \tag{4.16}$$

4.2.4. Flavor constraints

An analysis of LFV in the RSIII has been carried out in Ref. [46] for the case of fermionic DM, where bounds on the yukawa couplings have been derived. The results from a recent analysis of LFV processes in the minimal scotogenic model for fermion DM masses of up to 3 TeV [115] can be extended to the RSIII. These bounds, however, do not directly apply for our case, with significantly lighter NP fermions. In our model the yukawa couplings, which are obtained from the neutrino masses, turn out to be at most of order $\mathcal{O}(10^{-4})$ if we choose the orthogonal matrix R of Eq. (4.9) to be real. In this case the LFV bounds do not further constrain the available parameter space. On the other hand, if R is allowed to be complex, much larger values of the yukawa couplings can be obtained and the $\mu^+ \to e^+\gamma$ and $\tau \to \mu\gamma$ bounds [116, 117] restrict their largest values, of approximately 1 (0.5) for the electron yukawa in the normal (inverted) hierarchy, and of order of a few for the muon and tau yukawa couplings.

4.2.5. Dark Matter constraints

The DM relic density measured by Planck [118] [2] in units of the critical density and the normalized Hubble constant h is $\Omega^{exp.}_{\rm DM}h^2 = 0.1197 \pm 0.0022$ at 68% confidence level (CL). Allowing for other unknown sources for DM this measurement only imposes a upper bound on the NP contribution to $\Omega_{\rm DM}h^2$. In the numerical analysis we require that the relic density lies within a 2σ uncertainty of the measured central value, $\Omega_{\rm DM}h^2 = 0.1197 \pm 0.0044$. Whenever we relax this constraint to allow for additional DM sources we only require that $\Omega_{\rm DM}h^2 < 0.1241$.

With respect to direct DM searches, we use the 90% CL upper bound of the spin-independent DM-nucleon cross section $\sigma^{max}_{\rm SI}$ given by LUX [119]. Allowing for an under-abundance of DM this bound is rescaled as

$$\sigma_{\rm SI} < \xi^{-1}_{\rm DM}\sigma^{max}_{\rm SI} \ , \tag{4.17}$$

with $\xi_{\rm DM} = \Omega_{\rm DM}/\Omega^{exp.}_{\rm DM} < 1$ the ratio of the DM relic density of our model and the experimental central value obtained by Planck [118]. The lower DM density leads to a smaller sensitivity for direct detection and consequently to a larger upper limit on

[2] We have used the result for Planck TT+lowP of Ref. [118]. A tighter bound is given for Planck TT,TE,EE+lowP, which does not significantly alter our analysis.

the spin-independent DM-nucleon cross section. Here one assumes that all remaining unknown sources of DM do not contribute to the direct detection signal.

For indirect DM searches, we use the 95% CL upper bound of the thermally averaged cross-section obtained by Fermi-LAT [120] for dwarf spheroidal galaxies with the 6-year Pass-8 Limit. In order to account for the different annihilation channels of our DM candidate we normalize the corresponding bounds for $\langle\sigma v\rangle_X$, with $X = b\bar{b}, WW, ZZ, hh$, and select the strongest one. Allowing for an underabundance of DM this bound is rescaled as

$$\langle\sigma v\rangle_X < \xi_{\rm DM}^{-2}\langle\sigma v\rangle^{max} \ . \tag{4.18}$$

4.3. Scalar sector

As already discussed in the introduction, the scalar sectors of the RSIII and the IDM [92, 97, 121–126] are the same, with the addition of yukawa couplings to the $\mathbf{Z}_2$-odd fermions and leptons. Therefore, the RSIII allows for a suitable scalar DM candidate satisfying all model constraints in two regions: the low energy region, with a DM mass below the W gauge boson mass, and the high energy region, with scalar masses above 500 GeV. We focus on the first region, where direct production of the $\mathbf{Z}_2$-odd fermions with large cross-sections is possible. We consider DM masses up to 120 GeV for the low mass region in order to assess the LHC expectations in the region where the DM relic density is less than the one measured by Planck. It should be noted, however, that in our numerical analysis of Sec. 4.8 we only consider scenarios where the DM relic density corresponds to the observed value measured by the Planck collaboration [118].

The constraints from electroweak precision observables (EWPO) strongly restrict the masses of the heavier scalars. The χ-square for three degrees of freedom, χ^2_3, is obtained from the difference between the oblique parameters S, T and U, computed following Refs. [97–99, 103], and their best fit point from EWPO for the SM, Eq. (4.12). In Fig. 4.4 we show, for m_{H^0} between 45 GeV and 80 GeV, the allowed regions at 68% (green), 95% (yellow) and 99% (red) CL in the $(m_{A^0} - m_{H^\pm})$, $(m_{H^\pm} - m_{H^0})$ plane, corresponding, respectively, to $\chi^2_3 \leq 3.506$, $\chi^2_3 \leq 7.815$, and $\chi^2_3 \leq 11.345$. The two remaining free parameters of the scalar sector, λ_2 and λ_L, have no effect on the oblique parameters. Contours of constant $m_{A^0} - m_{H^0}$ are shown as dotted lines. The gray area in Fig. 4.4 corresponds to $m_{H^0} > m_{A^0}$, for which H^0 is not the DM candidate. The

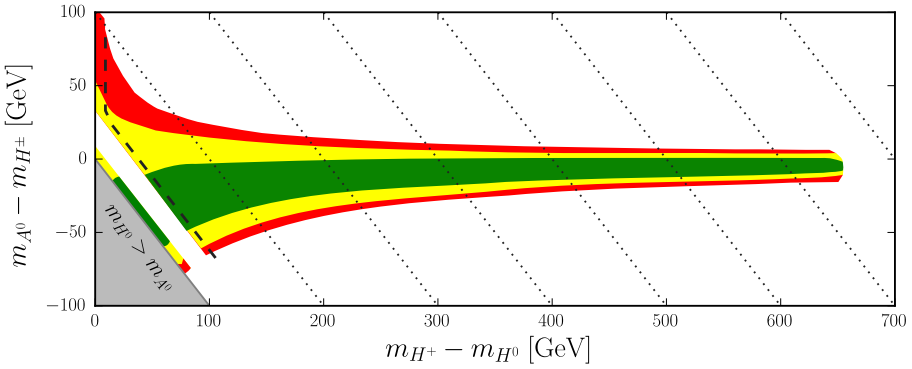

Figure 4.4.: EWPO constraints in the $(m_{H^+} - m_{H^0})$,$(m_{A^0} - m_{H^0})$ plane. The regions allowed at 68% (green), 95% (yellow) and 99% (red) CL have been obtained from the new physics contributions to the oblique parameters S, T, U. The dashed line delimits from below the region which allows for the correct scalar DM relic density in the RSIII. All shown points correspond to scenarios which satisfy the constraints of Sec. 4.2 for $m_{H^0} < 80$ GeV. The gray area corresponds to $m_{H^0} > m_{A^0}$, the dotted lines are contours of constant $m_{A^0} - m_{H^0}$.

stronger constraints come from T, which depends on the differences of masses between charged and neutral scalars, and S, which is sensitive to the difference of the neutral scalar masses. The dependence on m_{H^0} is weak but can be observed as a small overlap between the different CL regions in the low mass region. It should be noted that the contribution from the parameter U is often neglected, fixing $U = 0$ and evaluating the EWPO constraints with two degrees of freedom. In our case setting $U = 0$ leads to slightly narrower 68%, 95%, 99% CL allowed regions. The difference of the two choices is due to the fact that, while the central value of U and the contribution from the IDM to U are small, the correlation between the oblique parameters S, T and U is large (4.12).

In the allowed region where A^0 and $H^\pm$ decouple, with $m_{A^0}, m_{H^\pm} \gg m_{H^0}$, the heavy scalars are nearly degenerate. The upper bound on $m_{A^0} - m_{H^0}$ and $m_{H^\pm} - m_{H^0}$, of roughly 650 GeV, follows from the perturbativity constraints given in Sec. 4.2.1. In the region delimited to the left by a dashed line, the correct relic density can be obtained in the low mass DM regime, which excludes scenarios with small mass splittings between the DM candidate and the heavier scalars (see also the discussion on Fig. 4.5). Scenarios with $m_{A^0} - m_{H^0}$ between roughly 8 GeV and 30 GeV are further restricted by the LEP constraints on the second lightest neutral scalar, Eq. (4.13), within the range of DM masses considered here. In our analysis we have set conservatively $m_{A^0} > 110$ GeV.

For DM masses above 80 GeV the allowed range increases. For instance, for $m_{H^0} = 1$ TeV and $m_{H^\pm} \approx m_{H^0}$, the EWPO constrain $m_{A^0} - m_{H^\pm} \approx m_{A^0} - m_{H^0} \lesssim 110$ GeV at 95% CL instead of approximately $\lesssim 50$ GeV as in the low DM mass case. Requiring in addition for $m_{H^0} > 500$ GeV that these scenarios satisfy the measured relic density leads to $m_{A^0} - m_{H^0} \lesssim 12$ GeV and $m_{H^\pm} - m_{H^0} \lesssim 8$ GeV.

The constraints on the scalar sector from the thermal relic density measurements, direct and indirect detection, as well as the LHC, are analyzed performing a scan of the following parameters in the range

$$\begin{aligned} 45 \text{ GeV} < m_{H^0} < 120 \text{ GeV} , \\ 110 \text{ GeV} < m_{A^0} < 700 \text{ GeV}, \quad or \quad 0 < m_{A^0} - m_{H^0} < 8 \text{ GeV} , \\ 70 \text{ GeV} < m_{H^\pm} < 700 \text{ GeV}, \\ 10^{-5} < |\lambda_L| < |\lambda_L|^{max} , \end{aligned} \tag{4.19}$$

and fixed $\lambda_2 = 0.1$. The value of λ_2 is irrelevant for our study, as long as it fulfills the theory constraints. We have computed the spin-independent DM-nucleon cross section σ_{SI}, the thermal averaged annihilation cross-section $\langle \sigma v \rangle$ (4.18), and $R_{\gamma\gamma}$ (4.15) with the IDM model of micrOMEGAs (v4.1.8) [127]. We have confirmed these results comparing σ_{SI} and $\langle \sigma v \rangle$ with Ref. [93], and $R_{\gamma\gamma}$ following the treatment carried out in Ref. [128]. We also impose the EWPO, perturbativity of Sec. 4.2. The choice of parameters also satisfies the LEP collider constraints [109]. The value of $|\lambda_L|^{max}$ depends on the specific parameter point and is obtained from the perturbative unitarity constraint. All values of m_{A^0} and $m_{H^\pm}$ are below their perturbativity limit. The fermion sector has no effect on the DM observables due to the smallness of the yukawa couplings[3], not larger than $\mathcal{O}(10^{-4})$.

The result of the scan of parameters is shown in Fig. 4.5 in the relic density versus DM mass plane. Scenarios which fulfill all constraints are shown as green, dark green and light green dots. Dark green (light green) dots represent scenarios in which the main annihilation channel before freeze-out is the co-annihilation between A^0 and H^0 ($H^\pm$ and

[3] We have restricted our analysis to the case of real orthogonal matrix R (4.9). The solutions with large yukawa couplings obtained allowing R to be complex are highly fine-tuned [129]. The compatibility with the neutrino oscillation data [55], achieved through Eq. (4.9), receives large higher order radiative corrections [130] which spoil the fine-tuning obtained at leading order. It is worth noticing that, while new DM annihilation channels may become significant, allowing for new lighter scalar DM solutions, the experimental signatures from heavier $\mathbf{Z}_2$-odd fermion decays should not significantly modify our phenomenological analyisis, as can be inferred from SUSY searches.

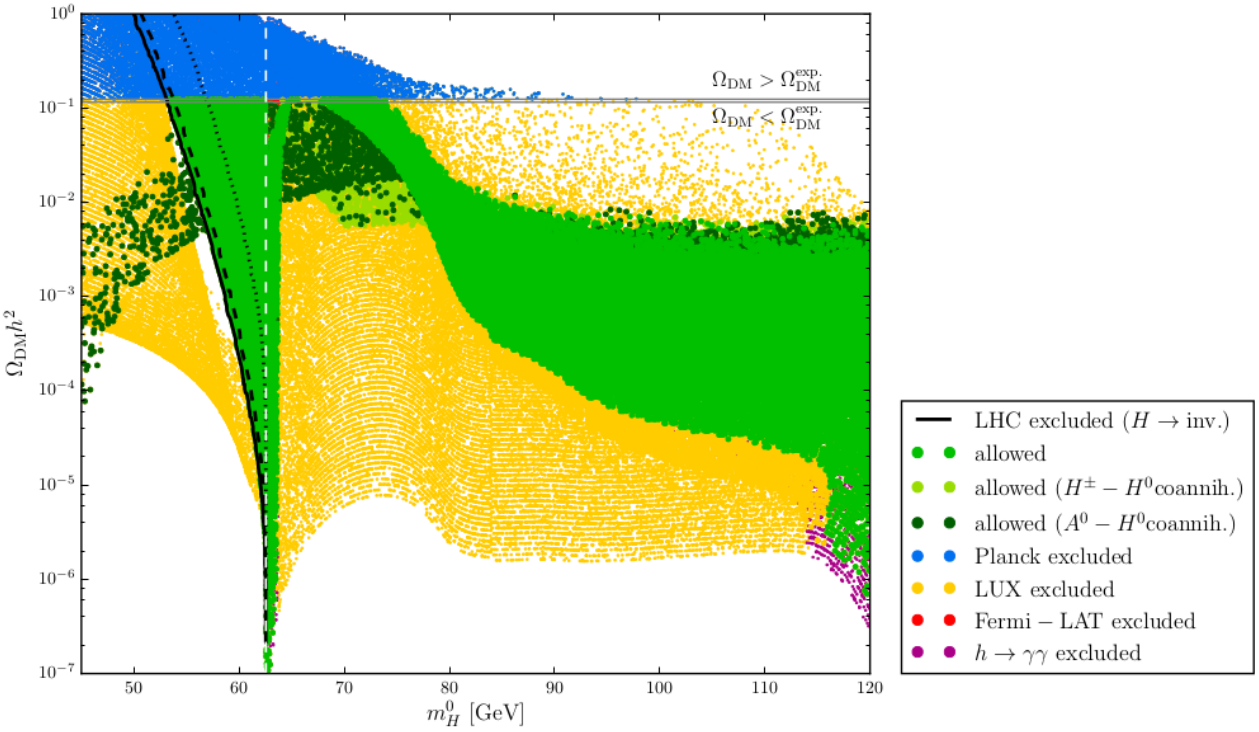

Figure 4.5.: Constraints of the scalar sector of the RSIII in the $\Omega_{\rm DM}h^2, m_{H^0}$ plane. Green points satisfy all constraints of Sec. 4.2. Dark green (light green) points represent scenarios with $m_{A^0} - m_{H^0} < 8$ GeV ($m_{H^\pm} - m_{H^0} < 12$ GeV), in which A^0–H^0 ($H^\pm$–H^0) co-annihilation is the dominant annihilation channel before freeze-out. The upper bound on the invisible Higgs decay width from the LHC (black curve) gives a lower bound on m_{H^0} except for the dark green points (H^0–A^0 co-annihilation scenarios). The remaining scenarios are excluded by Planck relic density measurement (light blue), LUX direct detection searches (yellow), Fermi-LAT indirect detection searches (red), LHC Higgs decay to photons (purple). The bound for the invisible Higgs decay for a naive projection at the LHC Run-II (ILC expected sensitivity) is shown as a dashed (dotted) black curve. The horizontal lines represent the 2σ band on the measured relic density. A vertical dashed gray line shows the threshold of Higgs decay to DM pairs.

H^0), defined here by $m_{A^0} - m_{H^0} < 8$ GeV ($m_{H^\pm} - m_{H^0} < 12$ GeV). The mass difference between the coannihilating scalars is small enough to avoid the Boltzmann suppression before freeze-out. As this mass splitting increases, the annihilation cross-section decreases, leading to a larger relic density. For instance, at low m_{H^0} the A^0–H^0 co-annihilation scenarios have a lower limit in $\Omega_{\rm DM}h^2$ when the splitting vanishes, and an upper limit when it reaches its maximum value of 8 GeV, implying that for low DM masses the coannihilation mechanism is too efficient to allow for the observed relic density. The dark green dots in the light green region for $m_{H^0} \approx 70$ GeV correspond to scenarios where both

heavier scalars coannihilate with H^0. For larger values of $\Omega_{\rm DM}h^2$ both co-annihilation regions overlap but the dark dots cover the light ones. Similarly, the green dots cover the light and dark ones where those regions overlap.

Scenarios excluded by the upper bound on the relic density measurement by Planck [118], Sec. 4.2.5, are shown in light blue. Scenarios with a smaller value of $\Omega_{\rm DM}h^2$ are not excluded but lead to an underabundance of DM which cannot fully account for the DM content of the Universe. In that case the direct detection upper bound on the spin independent cross-section σ_{SI}^{max} is rescaled with $\xi_{\rm DM}^{-1}$ as in Eq. (4.17) to take into account the smaller DM flux on the detector. Analogously, the indirect detection upper bound on the thermally averaged cross-section is rescaled with $\xi_{\rm DM}^{-2}$ as in Eq. (4.18). The upper bound on the relic density excludes scenarios without an efficient mechanism of annihilation before freeze-out. These scenarios are characterized by a large splitting between H^0 and the heavier scalars, suppressing the co-annihilation channels, and, for $m_{H^0} < M_W$ a small DM–Higgs coupling λ_L, suppressing the Higgs exchange channel, while for $m_{H^0} \approx M_W$, by $\lambda_L \sim \mathcal{O}(-0.1)$, leading to a destructive interference between different annihilation channels to gauge bosons. Also shown are the maximum and minimum allowed values for the relic density as measured by Planck at 95% CL level if one requires that the model fully explains the DM content of the Universe.

The strongest constraint from the LHC comes from the present bound on the invisible branching ratio of the Higgs boson, shown as a black solid line, which sets a lower mass limit for H^0 whenever the Higgs-portal is the main DM annihilation channel. For $\xi_{\rm DM} = 1$ this bound excludes $m_{H^0} < 53$ GeV. For $\xi_{\rm DM} < 1$ it excludes scenarios with masses of up to $m_h/2$, unless the H^0–A^0 co-annihilation channel contributes significantly to the total annihilation before freeze-out. In the later case, corresponding to the band of dark green points in the light DM mass region, the DM-Higgs boson coupling λ_L is small enough to restrict the invisible Higgs decay, while the co-annihilation channel ensures that the Planck upper limit on the relic density is fulfilled. Also shown as a black dashed line is the future projection of the upper limit on the invisible decay of the Higgs boson at Run-II of the LHC assuming a future limit for the invisible Higgs decays $\mathrm{Br}^{LHC13}(h \to inv.) < 0.065$ [111], and as a black dot-dashed line the corresponding prospect for the ILC with $\sqrt{s} = 1$ TeV and 1 ab^{-1} [131], $\mathrm{Br}^{ILC}(h \to inv.) < 0.0026$.

Scenarios allowed by Planck upper limit but excluded by the direct detection constraints from LUX [119] are shown in yellow. The lower sensitivity to the spin independent cross-section resulting when the relic density is smaller than the experimental measured value, obtained rescaling the upper limit with the factor the $\xi_{\rm DM}^{-1}$, reduces the excluded

region significantly. The direct detection limit also depends on variations on the local DM density, which would have to be included in the factor $\xi_{\rm DM}$. It is interesting that, for $\Omega_{\rm DM} = \Omega_{\rm DM}^{exp.}$, the lower bound on m_{H^0} from LUX is only slightly stronger than that from the invisible Higgs decay. For $\Omega_{\rm DM} = \Omega_{\rm DM}^{exp.}$ LUX also sets the upper limit $m_{H^0} < 74$ GeV, corresponding to scenarios with $\lambda_L \approx -0.012$. Larger values of m_{H^0} require larger values of $|\lambda_L|$ in order to obtain the correct relic density, increasing the spin independent cross-section above the LUX bound. Allowing for DM underabundance LUX constrains regions of parameter space up to $m_{H^0} = 120$ GeV. For $m_{H^0} > 110$ GeV and $\lambda_L \neq 0$ the Higgs pair-production channel becomes a relevant annihilation channel, further reducing the relic density and relaxing the constraints due to the rescaling of the bounds.

The indirect detection constraint from Fermi-LAT [120], shown in red, does not exclude any region of parameter space allowed by the relic density upper limit [118] after we rescale the thermally averaged cross-section by $\xi_{\rm DM}^{-2}$. A small region with $\Omega_{\rm DM} \approx \Omega_{\rm DM}^{exp.}$ and $m_{H^0} \gtrsim m_h/2$, in the funnel region, is only allowed if the splitting between A^0 and H^0 is small and the co-annihilation channel opens up before freeze-out.

Once all DM constraints are imposed the LHC measurement of the ratio of the observed diphoton production cross section relative to the SM expectation [112] constrains a small region of the parameters with $m_{H^0} \gtrsim 114$ GeV and a very small value of relic density.

For 120 GeV $< m_{H^0} <$ 500 GeV, where the model leads to an underabundance of DM, the Higgs diphoton decay restricts a small region in relic density versus DM mass plane with very small relic density, corresponding to large λ_L and light $H^\pm$.

4.4. Phenomenology

In this section we analyze the phenomenological implications of the constraints on our model given in Sec. 4.1 in order to select representative benchmark scenarios for LHC searches.

Although the $\mathbf{Z}_2$-odd fermion sector of the RSIII has the same gauge quantum numbers as the Type III Seesaw model [15], the limits obtained for the latter by ATLAS [21] and CMS [132, 133] cannot be interpreted as limits in our model due to its $\mathbf{Z}_2$ symmetry, which forbids the decay of the $\mathbf{Z}_2$-odd fermions to SM particles.

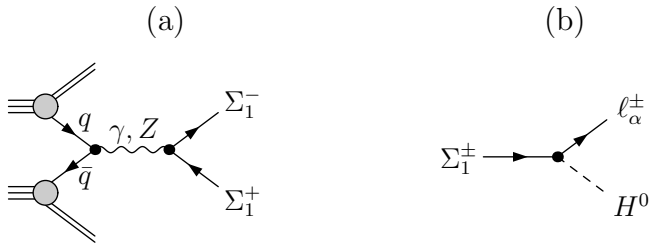

Figure 4.6.: The left panel (a) shows the main production channel for pair $\Sigma_1^-\Sigma_1^+$ at the LHC. The right panel (b) shows the main decay channels of $\Sigma_1^\pm$ to DM. Here q denotes quarks of the first generation and $\ell_\alpha = e, \mu, \tau$.

The main production channel of lighter $\mathbf{Z}_2$-odd fermions at the LHC is shown in Fig. 4.6a. At the LHC gauginos are produced via the s-channel exchange of a gauge boson and via t-channel exchange of a left-handed squark. Since the gauge structure of the $\mathbf{Z}_2$-odd fermions and that of charginos and neutralinos in the pure gaugino limit is the same, their gauge couplings are also equal. Therefore, the production cross-section of $\mathbf{Z}_2$-odd fermions at the LHC can be obtained from that of charginos and neutralinos in the pure gaugino limit with decoupled sfermions, where the t-channel can be neglected. For large values of the supersymmetric Higgsino parameter μ we have checked that the Higgsino component of the chargino is negligible and that the results are independent of its value. We restrict our analysis to the lightest family, Σ_1, for which one obtains the largest production cross-section of $\mathbf{Z}_2$-odd fermion pairs, $pp \to \Sigma_i^+\Sigma_i^-$, $i = 1, \ldots, n_\Sigma$. Our conclusions should be easily extended to the heavier $\mathbf{Z}_2$-odd fermions. Notice that two-body decays from the heavier $\mathbf{Z}_2$-odd fermions to the lighter ones are forbidden because the mixing mass matrix M_Σ is diagonal.

At tree level the $\mathbf{Z}_2$-odd fermions decay via yukawa interactions to a $\mathbf{Z}_2$-odd scalar and lepton. The yukawa couplings are obtained varying the free neutrino parameters and applying the Casas-Ibarra prescription, Eq. (4.9). In the simplest scenario only H^0 is lighter than the fermion, with the heavier scalars A^0 and $H^\pm$ decoupled and nearly degenerate. In this case, shown in Fig. 4.6b, both fermions decay exclusively to a lepton and the DM candidate,

$$\Sigma_1^\pm \to \ell_\alpha^\pm H^0 \quad (\ell_\alpha = e, \mu, \tau) \ , \tag{4.20}$$

resulting in final state dileptons plus MET. This channel is expected to be the "best case scenario" for $\mathbf{Z}_2$-odd fermion searches at the LHC. Neglecting the lepton masses the branching ratios for the decay of the $\mathbf{Z}_2$-odd lepton are proportional to the absolute

square of the normalized yukawa couplings,

$$\mathcal{B}_\alpha \equiv \mathrm{Br}(\Sigma_1^\pm \to \ell_\alpha H^0) = |\hat{Y}_\alpha|^2 \ . \tag{4.21}$$

The $\mathbf{Z}_2$-odd fermion pair-production channel with the largest production cross-section is $\Sigma_1^0\Sigma_1^\pm$. However, Σ_1^0 decays exclusively to the invisible final state $\nu_\alpha H^0$, leading to a final state with only one charged lepton and will not be considered here. Notice that in the Type III Seesaw model, which has the same fermionic content, the decay chains are different due to the absence of a discrete symmetry, leading to different collider signatures [20].

If more than one scalar is lighter than the $\mathbf{Z}_2$-odd fermion, new decay channels to unstable particles open up,

$$\Sigma_1^\pm \to \ell_\alpha^\pm A^0, \quad \Sigma_1^\pm \to \nu_\beta H^\pm, \quad (\ell_\alpha = e,\mu,\tau;\ \nu_\beta = \nu_e,\nu_\mu,\nu_\tau) \ , \tag{4.22}$$

followed by the secondary decays

$$A^0 \to H^0 Z, \quad H^\pm \to H^0 W^\pm \ , \tag{4.23}$$

as well as the subleading decays $A^0 \to H^\pm W^\mp$ or $H^\pm \to A^0 W^\pm$. The gauge boson of the secondary decays may be on-shell or virtual, depending on the mass spectrum. In addition, the $\Sigma_1^\pm\Sigma_1^0$ production channel may lead to final states with at least two leptons, of either opposite sign or same sign,

$$pp \to \Sigma_1^\pm \Sigma_1^0, \quad \Sigma_1^\pm \to \ell_\alpha^\pm A^0/H^0, \quad \Sigma_1^0 \to \ell_\beta^\mp H^\pm \quad (\ell_\alpha,\ell_\beta = e,\mu,\tau) \ , \tag{4.24}$$

followed by the secondary decays of Eq. (4.23). Not shown in (4.24) are the decays to a neutrino and a scalar. The partial decay width of the decays of Eq. (4.24) is given by

$$\Gamma(\Sigma_1 \to \ell_\beta \Phi^0) = \frac{|Y_{1\beta}|^2}{64\pi}\frac{(m_{\Sigma_1}^2 - m_{\Phi^0}^2)^2}{m_{\Sigma_1}^3}, \quad \Phi^0 = H^0, A^0 \ , \tag{4.25}$$

$$\Gamma(\Sigma_1^0 \to \ell_\beta^\pm H^\mp) = \frac{|Y_{1\beta}|^2}{32\pi}\frac{(m_{\Sigma_1}^2 - m_{H^\pm}^2)^2}{m_{\Sigma_1}^3} \ . \tag{4.26}$$

If all scalars are lighter than $\Sigma_1^\pm$ and nearly degenerate the branching ratios for $\Sigma_1^\pm$ decaying to H^0, A^0 and $H^\pm$ tend to the asymptotic values 1/4, 1/4 and 1/2, respectively.

4.5. Collider limits

Processes with electroweak pair-production and decay of $\mathbf{Z}_2$-odd particles at colliders, and in particular at the LHC, have been extensively studied in the framework of supersymmetry. Those searches can be interpreted in the framework of the RSIII to constrain this model. The pair-produced $\mathbf{Z}_2$-odd particles cascade further to the LOP, leaving similar collider signatures as those searched for. The most convenient way to analyze those results are simplified model spectra analyses, where limits on the production cross-sections for NP searches are given as a function of the spectrum.

We focus on a set of benchmark scenarios with well defined decay topologies and compare these results to LHC searches for supersymmetric processes. The simplest decay topology is that in which both $\mathbf{Z}_2$-odd fermions decay to the DM candidate, Eq. (4.20), leading to a collider signature of hard opposite sign leptons plus MET. Both slepton and chargino pair-production and decay can lead to similar final state topologies. Pair-production of left-handed sleptons, where each slepton decays further to the lightest neutralino and a lepton of the first two families, $pp \to \tilde{\ell}_L \tilde{\ell}_L \to \ell^\pm \ell^\mp \tilde{\chi}_1^0 \tilde{\chi}_1^0$, with $\ell = e, \mu$ and $\tilde{\chi}_1^0$ the lightest neutralino, leads to a collider signature of OSSF leptons plus MET. The case of stau production will be considered separately. In the RSIII the flavor structure for the final leptons is in general different. In the special e-philic or mu-philic cases, where the lightest $\mathbf{Z}_2$-odd fermions decay exclusively to electrons or muons, respectively, we can extrapolate the observed exclusion limit by ATLAS for left-handed slepton pair-production [50] assuming that the detection efficiency of the most sensitive SR remains constant up to higher mass scales. Taking into account the larger production cross-section for the fermions one can estimate the lower mass exclusion limit $m_{\Sigma_1^\pm} > 630$ GeV. In chargino pair-production, each chargino decays to a lepton and a slepton, which decays further to a secondary lepton and a neutralino. This process may lead to leptons of different flavor but the final state has two additional neutrinos and in general softer leptons, depending on the chosen intermediate slepton masses. Experimental signatures of dileptons plus MET are also obtained in chargino-neutralino production decaying further via sleptons, $pp \to \tilde{\chi}_1^\pm \tilde{\chi}_2^0 \to \ell^\pm \ell'^+ \ell'^- \tilde{\chi}_1^0 \tilde{\chi}_1^0$, when one of the final leptons is not detected. In this case both same flavor and opposite flavor leptons are expected[50].

Among the several high energy physics tools have been developed which allow to reinterpret the results from the experimental collaborations at the LHC we have chosen the package `CheckMATE` [56–58], which allows to obtain exclusion limits on simplified

models of NP based on an increasing number of ATLAS and CMS analyses. This package applies to the events generated by the user the same selection cuts as in each of the included analyses by the experimental collaborations using the fast detector simulator DELPHES [134]. Subsequently, making use of the CL_s prescription [135, 136] on the most sensitive SR, it establishes whether a given point under evaluation is ruled out or not based on the data given by the collaborations in their published analyses. The implementation of the model in HEP tools is described in more detail in Sec. 4.7. The most accurate exclusion results are expected for processes with the same production and decay topologies, as well as similar production cross-sections, as those in the supersymmetric searches reported in the included experimental analyses. Notice that the cuts in the experimental analyses have been optimized for the mass range where the exclusion limits are found.

If more than one NP scalar is lighter than the produced fermions, additional decay channels open up, Eqs. (4.22)-(4.24), for which there is no analogous supersymmetric process with similar decay topologies. The heavier scalars decay further, dominantly to a gauge boson and the DM candidate. This secondary decay leads to large hadronic activity and is not expected to improve the exclusion sensitivity in any of the processes included in `CheckMATE` . Most of the events with the additional topologies should not pass the selection cuts of the LHC analyses, which are optimized to reject additional hadronic activity. Therefore, the number of selected events should decrease as the branching ratios of the new decay channels increase. It is then natural to define a "best case scenario", where the $\mathbf{Z}_2$-odd fermions are the NLOP and all other NP particles are heavier, and a "worst case scenario", where all NP scalars are light and nearly degenerate. In the latter case the branching ratio of Σ_1^+ to the heavier scalars approaches 75%. It should be noticed, however, that a minimal mass splitting with the DM candidate is necessary in order to avoid a very large contribution of the co-annihilation channel in the early Universe.

In the intermediate case, in which the decay A^0 and $H^\pm$ are kinematically open but significantly heavier than H^0, the decay to the DM candidate will be enhanced with respect to the other channels. Since the mass splitting of the two heavier scalars is strongly bounded by EWPO the above mentioned cases cover most of the allowed parameter space.

Within each of the benchmark scenarios discussed, the decay to leptons of the first two families has the highest sensitivity. The case when the $\mathbf{Z}_2$-odd fermions decay predominantly to taus, which have small branching ratios to leptons, is not expected to

lead to a significant exclusion in our analysis with `CheckMATE` , for which no experimental analyses have yet been included in this package. This case will be considered separately, reinterpreting the stau search analysis reported in Ref. [54].

In more realistic scenarios, f.i. in cases where the decay process involves several final state topologies, only the SR with the largest expected sensitivity is considered. It is possible, however, to combine those SRs and improve the exclusion limits using the CL_s method [135, 136].

4.6. Combination strategy

In each of the decay channels, defined by their experimental signature of hard e^+e^-, $\mu^+\mu^-$, and $e^\pm\mu^\mp$ plus MET, we identify the most sensitive SR. Since the flavor of the leptons depends on the unknown yukawa couplings a realistic analysis should allow for its whole range. In the range of masses we are considering this SR turns out to be SR–$\mathrm{m_{T2,110}}$ of Ref. [50], except for $m_{\Sigma^\pm} \approx 350$ GeV, where SR–$\mathrm{m_{T2,110}}$ and SR–$\mathrm{m_{T2,90}}$ have similar sensitivities. We have chosen to use only the former SR. The eventual small loss in sensitivity can be regarded as conservative.

Assuming that the three dileptonic channels are uncorrelated, and thus statistically independent, we combine these channels using the CL_s method [135, 136], taking into account for the uncertainty on the background as in Ref.[137]. Details about our implementation of the CL_s method are given in Appendix A. We neglect the uncertainty on the signal since it is much smaller and therefore its effect should be subleading. The uncertainty due to the statistics of the Monte Carlo simulations has been ignored, as it can be eventually reduced with larger samples [20]. The combination is expected to lead to stronger exclusion limits whenever more than one channel contributes to the final dileptons. It should be noticed that we cannot combine the decay channels with decays to taus.[4]

4.7. Implementation of the model in Heptools

The model has been implemented in the `Mathematica` package `FeynRules` (v2.0) [138] where the derivation of the complete set of Feynman rules from the Lagrangian given

[4] The charged leptons in the final state used in the SRs of of Ref. [50] are either electrons or muons.

in Eq. (4.1) are performed. The model files obtained from FeynRules are exported to micrOMEGAs (v4.1.8) [127] where DM observables are evaluated. The model is then exported in the Universal FeynRules Output (UFO) format to the parton-level Monte Carlo (MC) generator MadGraph (v5.2.2.3) [139]. The signal events are generated at $\sqrt{s} = 8$ TeV, without cuts in the run cards, where a total of 30K of events per point in the parameter space is simulated. The MC samples incorporate the NNLO [140] parton distribution functions (PDF). MadGraph is interfaced with Phythia (v6.4) [141], which simulates the parton showering and hadronization. In order to evaluate the production cross-section $pp \to \Sigma_i^+ \Sigma_i^-, i = 1, 2, 3$, we compute the chargino pair-production in the pure gaugino limit with a modified version of prospino [142], at next to the leading order (NLO) in α_s, where we have set to zero the chargino-quark-squark couplings in order to eliminate the t-channel contribution. Finally the signal samples and their corresponding NLO cross-sections are passed to CheckMATE (v1.1.15) [56–58], where the samples pass thought a fast detector simulator DELPHES (v3.0)[134], which uses FastJet [143] with the anti-kT algorithm [58] for particle reconstruction.

4.8. Numerical results

We define two benchmark scenarios which satisfy all constraints discussed in Sec. 4.2, the "best case scenario" ($\mathcal{S}_\mathcal{B}$), with decoupled heavier scalars, and the "worst case scenario" ($\mathcal{S}_\mathcal{W}$), with nearly degenerate scalars,

$$\begin{aligned} \mathcal{S}_B: &\quad m_{H^0} = 70 \text{ GeV}, \; m_{H^\pm} = 700 \text{ GeV}, \; m_{A^0} = 700 \text{ GeV}, \\ \mathcal{S}_W: &\quad m_{H^0} = 60.2 \text{ GeV}, \; m_{H^\pm} = 70.4 \text{ GeV}, \quad m_{A^0} = 110.0 \text{ GeV}. \end{aligned} \tag{4.27}$$

The DM relic density lies within the measured range by Planck [118], $\Omega_{DM}h^2 = 0.1197 \pm 0.0044$. The mass of the lightest $\mathbf{Z}_2$-odd charged fermion varies between its LEP lower limit, Eq. (4.13), and 700 GeV. The two heavier $\mathbf{Z}_2$-odd fermion triplets, which are not phenomenologically relevant, are set to 1.5 TeV and 2.5 TeV, respectively. Since the yukawa couplings of the $\mathbf{Z}_2$-odd fields are related to the underlying mechanism of neutrino mass generation, a realistic phenomenological analysis of the RSIII should also study the flavor structure of the model. We define the following extreme cases for the normalized yukawa couplings to the lightest $\mathbf{Z}_2$-odd fermions: e-phobic ($\hat{Y}_1 = 0$), mu-phobic ($\hat{Y}_2 = 0$), e-mu-symmetric ($\hat{Y}_1 = \hat{Y}_2 \leq 1/\sqrt{2}$), and tau-philic ($\hat{Y}_1 \approx 1$), which should be regarded as simplified models in flavor space.

4.9. Best case scenario

Within our benchmark scenario with decoupled heavier scalars, $\mathcal{S}_B$, we have generated random parameter-sets for which the neutrino constraints are satisfied, and where the lightest $\mathbf{Z}_2$-odd fermion mass, $m_{\Sigma_1^\pm}$, lies within the allowed range. The most relevant parameters are $m_{\Sigma_1^\pm}$, which determines the production cross-section at the LHC, and the normalized yukawa couplings of the triplet fermions, $\hat{Y}_\alpha$, with $\alpha = 1, 2, 3$, which fully determine the tree-level branching ratios $\mathcal{B}_\ell$, with $\ell = e, \mu\, \tau$.

The implementation of our model in high energy physics tools has been described in Sec. 4.7. For each parameter-set we generated events for our process at 8 TeV center of mass energy, $pp \to \Sigma_1^+\Sigma_1^-$ followed by $\Sigma_1^\pm \to H^0\ell^\pm$. We obtain with CheckMATE the exclusion CL in each of the three most sensitive SRs, SR–$\mathrm{m_{T2,110}}$ in the channels e^+e^-, $\mu^+\mu^-$, $e^\pm\mu^\mp$ plus MET, as well as the number of background, observed and signal events which pass all the cuts of that experimental search [50]. With the latter we compute the combined exclusion confidence level with the $C\mathrm{L}_s$ method described in Sec. 4.6. For e-philic and mu-philic scenarios we have checked that both methods are consistent within the numerical uncertainties, which in the $C\mathrm{L}_s$ method strongly depends on the numerical integration and on the background uncertainty.

We focus on regions of parameter space for which the exclusion CL lies above 90%. In Fig. 4.7 we show the 95% CL exclusion contours in the $\mathcal{B}_e$,$\mathcal{B}_\mu$ plane (panel a) and in the $\mathcal{A}_{e\mu}$, $(\mathcal{B}_e - \mathcal{B}_\mu)$ plane (panel b), with $\mathcal{A}_{e\mu} = (\mathcal{B}_e - \mathcal{B}_\mu)/(\mathcal{B}_e + \mathcal{B}_\mu)$. The contours in the 95% exclusion CL have been obtained fitting $\mathcal{A}_{e\mu}$ as a function of $(\mathcal{B}_e + \mathcal{B}_\mu)$ with a quartic polynomial. The regions above the corresponding curves are excluded. Changing the order of the fitted polynomial we conclude that the uncertainty in these fits turns out to be larger for $\mathcal{A}_{e\mu} = \pm 1$. As expected, for a given fermion mass the strongest exclusion is obtained for the mu-phobic case, with $\mathcal{A}_{e\mu} = 1$, followed by the mu-philic case, with $\mathcal{A}_{e\mu} = -1$. In the e, μ symmetric case, with $\mathcal{A}_{e\mu} = 0$ and $\mathcal{B}_e = \mathcal{B}_\mu$, the exclusion sensitivity is reduced since only half of the events without taus lead to OSSF leptons, which fall into the most sensitive SRs, while the other half of those events lead to OSDF leptons. Shown as a star is the flavor symmetric case, in which all three branching ratios are equal. As the branching ratios to taus increase, the exclusion sensitivity decreases, since most of these events are lost in the analysis, resulting in a smaller fermion mass exclusion. F.i., for $\mathcal{B}_\tau = 1 - \mathcal{B}_e - \mathcal{B}_\mu \approx 0.85$, ATLAS [50] excludes $m_{\Sigma_1^\pm} \lesssim 350$ GeV, corresponding to the $m_{\Sigma^\pm} = 350$ GeV contour on the lower part of Fig. 4.7b. It should be noted that these results alone do not constitute solid lower mass

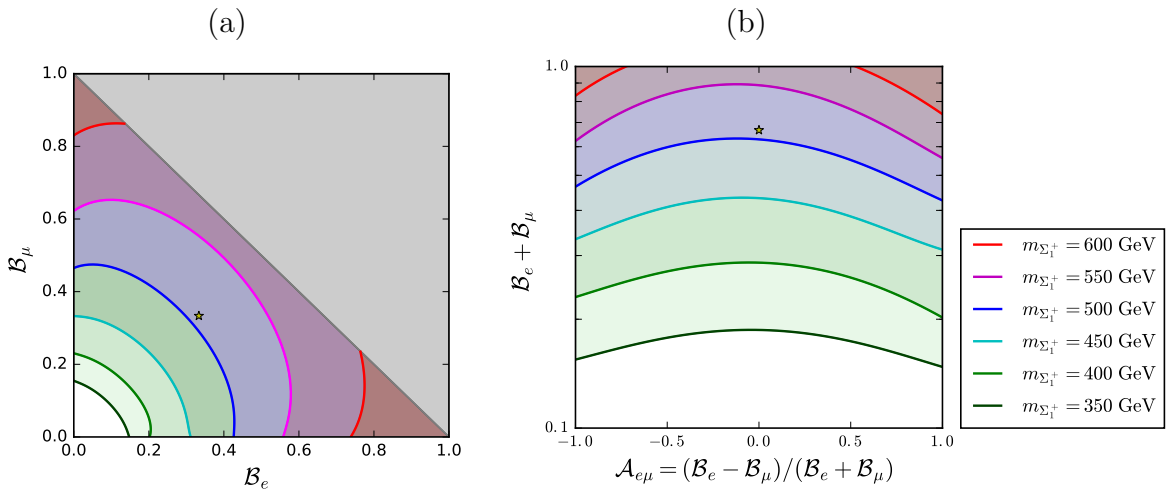

Figure 4.7.: Contours of constant $m_{\Sigma_1^+}$ for the present LHC exclusion sensitivity of the RSIII in the $\mathcal{B}_e, \mathcal{B}_\mu$ plane (a) and $\mathcal{A}_{e\mu}, (\mathcal{B}_e + \mathcal{B}_\mu)$ plane (b), for $m_{H^0} = 70$ GeV and $m_{H^\pm} \approx m_{A^0} > m_{\Sigma_1^\pm}$. The flavor symmetric scenario with $\mathcal{B}_e = \mathcal{B}_\mu = \mathcal{B}_\tau$ is shown with a star. The shaded triangle in (a) is not physical. Both figures show the same results. In (b) the area above each contour is excluded for the corresponding NP fermion mass.

limits for the fermions (as a function of their yukawa couplings) since the experimental analysis does not cover the region with compressed spectra. We target the parameter region with small $\mathbf{Z}_2$-odd fermion masses at the end of this section reinterpreting a search for electroweak supersymmetric searches in the regions of compressed spectra. For consistency we have checked the exclusion limits obtained with CheckMATE for small $\mathbf{Z}_2$-odd fermion-scalar mass splitting, where most decay leptons fail to have sufficient p_T to pass the experimental cuts. Here we set $m_{H^0} = 70$ GeV as in $\mathcal{S}_B$. In the most sensitive e-philic case we can exclude $m_{\Sigma_1} > 135$ GeV, i.e. with a mass splitting larger than 65 GeV, while for $\mathcal{B}_\tau = 0.85$, $\mathcal{B}_e = 0.15$ this mass limit increases to $m_{\Sigma_1} > 155$ GeV. Similar results are obtained for the e-phobic case.

The results obtained from Fig. 4.7 for $\mathcal{A}_{e\mu} = -1$, $\mathcal{A}_{e\mu} = 0$, and $\mathcal{A}_{e\mu} = 1$ are shown in Fig. 4.8, where $\mathcal{B}_e - \mathcal{B}_\mu$ is plotted as a function of $m_{\Sigma_1^\pm}$. One observes that in the e-mu-symmetric case, corresponding to $\mathcal{A}_{e\mu} = 0$, the mass limit is reduced by up to 50 GeV for large masses, down to approximately 20 GeV for the smaller masses. In the mu-phobic case we obtain the highest exclusion sensitivity, excluding masses of Σ_1 of up to approximately 660 GeV. Recently ATLAS has performed a dedicated analysis [54] to target compressed spectra, as well as decays with final tau leptons The bounds on sleptons can be reinterpreted in our model in the e-philic, mu-philic and tau-philic limits

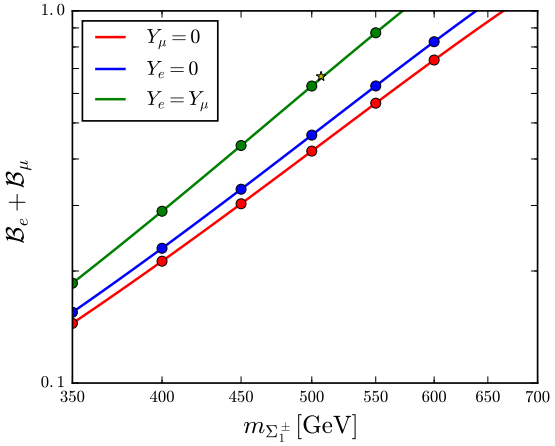

Figure 4.8.: Present LHC exclusion sensitivity in the $m_{\Sigma_1^+}$, $(\mathcal{B}_e + \mathcal{B}_\mu)$ plane for $m_{H^0} = 70$ GeV and $m_{H^\pm} \approx m_{A^0} > m_{\Sigma_1^\pm}$, in the mu-phobic (red), e-phobic (blue) and e-mu-symmetric (green) scenarios. The flavor symmetric scenario with $\mathcal{B}_e = \mathcal{B}_\mu = \mathcal{B}_\tau$ is shown with a star. The region above each curve is excluded.

taking the larger production cross-sections of the $\mathbf{Z}_2$-odd fermions into account, since both the stau decay, $\tilde{\tau}_1 \to \tau^- \tilde{\chi}_1^0$ and $\Sigma_1^- \to \tau^- H^0$, lead to the same experimental signature. In the DM region relevant for our study, with $m_{\tilde{\chi}_1^0}$ between 50 and 70 GeV, the bounds on direct stau production are not yet strong enough to reach the exclusion level. However, rescaling the cross-section, one can safely exclude $m_{\Sigma_1^\pm}$ between the LEP bound of 103.5 GeV and 300 GeV, as shown in Fig. 4.9 for $m_{H^0} = 60$ GeV and $m_{H^0} = 80$ GeV. For smaller m_{H^0} these limits are stronger, allowing to extrapolate our results to the whole scalar mass range. Assuming that the excluded cross-section for $m_{\Sigma_1^\pm} = 300$ GeV can be extrapolated to higher masses, implying that the sensitivity of this analysis remains constant, this limit can be extended to exclude fermion masses below approximately 400 GeV. Note that there is also a CMS [59] analysis with an even better exclusion limits in tau lepton, however for a direct comparison the ATLAS analysis was easier for the recasting. The CMS present the result for $m_\chi^0 = 1$ GeV, instead ATLAS present the exclusion limit for several values of m_χ^0, among them, a few ones, corresponding to a H^0 in the low mass DM regime.

For sleptons of the first two generations the slepton exclusion sensitivity is significantly stronger, allowing to exclude significant regions of parameter space [54]. Therefore, we can safely extend the limits obtained for the tau-philic case to the most general flavor structure. We conclude that all light $\mathbf{Z}_2$-odd fermion masses not covered by our previous

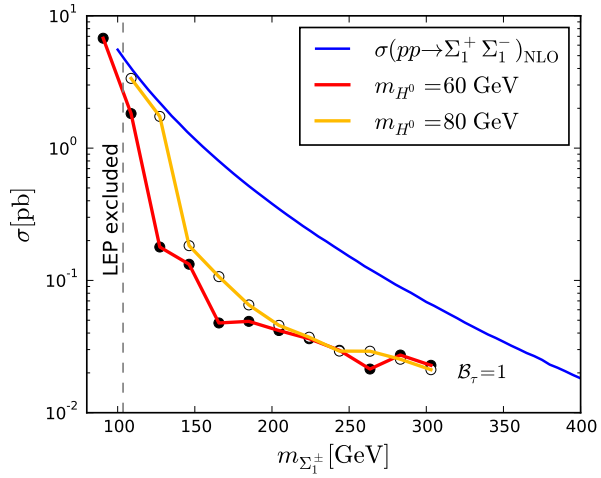

Figure 4.9.: NLO production cross-section for charged $\mathbf{Z}_2$-odd fermion pairs at the LHC with 8 TeV center of mass energy (blue line) as a function of the fermion mass. The corresponding 95% CL exclusion limits for the tau-philic case, when they decay exclusively to a tau and the DM scalar, are shown for $m_{H^0} = 60$ GeV (red line, black dots) and 80 GeV (yellow line, white dots). The limits have been obtained from those derived in [54] for stau pair-production. Also shown is the LEP lower bound on $m_{\Sigma_1^\pm}$.

analysis with CheckMATE can be excluded, so that the exclusion limits obtained in Fig. 4.8 are solid lower mass exclusion limits for our simplified model scenario.

4.10. Worst case scenario

The "worst case scenario" ($\mathcal{S}_\mathcal{W}$), Eq. (4.27), has been chosen such that the heavier scalars are lighter than the produced $\mathbf{Z}_2$-odd fermions, opening additional production and decay channels at the LHC. For a sufficiently large mass splitting between the fermion triplet and the scalars the branching ratios to the two neutral scalars approach 25%, and that of the charged scalar, the remaining 50%. For instance, for $m_{\Sigma_1^\pm} = 350$ GeV one obtains

$$\sum_{\ell=e,\mu,\tau} \mathrm{Br}(\Sigma_1^\pm \to \ell^\pm H^0 \mid A^0 \mid H^\pm) = 0.253 \mid 0.234 \mid 0.512 \,, \tag{4.28}$$

i.e. very close to the asymptotic values.

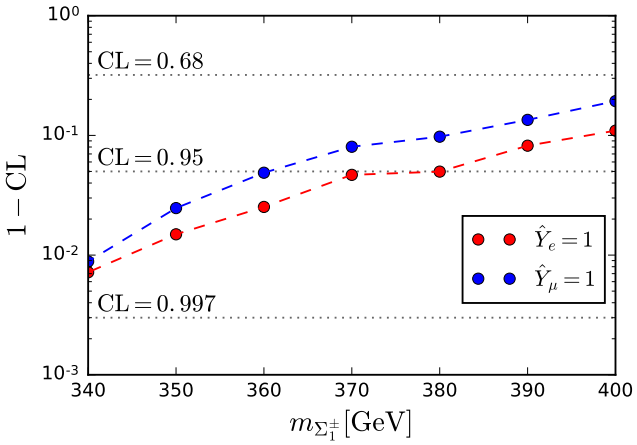

Figure 4.10.: Exclusion confidence level CL as a function of the NP fermion mass in the "worst case scenario" of Eq. (4.27). The dots correspond to the e-philic case $\hat{Y}_e = 1$ (red), mu-philic case $\hat{Y}_\mu = 1$ (blue). The dashed lines simply connect the dots. Masses for which $1 - \mathrm{CL} < 0.05$ are excluded.

Adding to the previously considered decay chain (4.20) the new decay chains of the $\mathbf{Z}_2$-odd fermions, Eqs. (4.22,4.23), could in principle lead to new significant experimental signatures. In our analysis with `CheckMATE` , however, those channels also lead to additional hadronic activity in the final state. We observed that the experimental cuts are effective in excluding most of these events, resulting in only a small number of new signal events from those channels. The overall effect on the exclusion CL is small, increasing the excluded mass by less of 20 GeV, while the computational effort turns out to be very large. Therefore we have neglected the new decay channels, resulting in a slightly smaller exclusion sensitivity, and only consider the decay to the DM candidate as in the "best case scenario".

We focus here on the e-philic and mu-philic cases of scenario $\mathcal{S}_W$, where the exclusion CL can be obtained directly from `CheckMATE` . In Fig. 4.10 we show the exclusion CL obtained with CheckMATE varying $m_{\Sigma_1^\pm}$ between 340 and 400 GeV. Only one scenario for each fermion mass has been computed here. We observe that, retaining only around 25% of the events, the masses of between 360 GeV for the mu-philic case, and 380 GeV for the e-philic case.

Chapter 5.

Conclusions

In order to account for the direct phenomenological inconsistencies which shown that the standard model (SM) is not the final theory in Nature, we exploit the realizations of the Weinberg operator in the SM, at the one-loop level and in the $SU(4)_L \otimes U(1)_X$ electroweak extension of the SM, at the tree level. For the latter case, mechanisms for neutrino mass generation is explored through the tree level realization of a Weinberg like operator in the $SU(4)_L \otimes U(1)_X$ extension. For four three-family models (models in which number fermion generations in Nature is explained) a systematic classification of the tree level realization of a Weinberg like operator is done. Two main topologies arises, one in which the intermediate particle is a fermion, either singlet or 15-plet of $SU(4)_L$ and a second one in which the intermediate particle is a scalar, either a decuplet or a 15-plet of $SU(4)_L$. For the so-called model F the canonical seesaw mechanism and the type-II like seesaw mechanism are implemented. For the latter, in the limit in which $\langle H_3^0 \rangle$ is small, the model predicts that the mixing matrix of the lightest neutrinos (the SM ones) and the heaviest neutrinos is exactly the same. Implying also that the mass ordered of the neutrinos in both sectors is exactly the same. In the SM, the one loop realization of the Weinberg operator led to an infinite set of models. By imposing that the particles propagating inside the loop transform non-trivially under a $\mathbf{Z}_2$ discrete symmetry, while all the other SM particle transforms trivially, then the lightest electrically neutral particle charge under $\mathbf{Z}_2$ is a natural DM candidate. From the set of potential models that posses a viable DM candidate as well as provide a correct description for the neutrino oscillation phenomena, the radiative type III seesaw model (RSIII) stands as one that also posses interesting LHC signatures worth of being explored. We have explored the RSIII, a scotogenic model in which an additional scalar doublet and at least two fermion triplets of $SU(2)_L$, odd under a conserved $\mathbf{Z}_2$ global symmetry, are added to the SM. This model has a natural DM candidate, the LOP, and radiatively generates the neutrino

masses by an effective Weinberg operator. We have focused in the low mass scalar DM region, where the LOP is a viable DM candidate satisfying all present theoretical and experimental constraints. In this region of parameter space the $\mathbf{Z}_2$-odd fermion triplets can have masses above the LEP limit for wino-like charginos, potentially leading to new physics signatures at the LHC. In order to set solid exclusion limits on the model we identify two extreme scenarios, a "best case scenario" where only the DM candidate is lighter than the fermion triplet, and a "worst case scenario" where all scalars are light. In the former, the decay process has simple decay topologies, which have been already studied in simplified model spectra analyses of supersymmetric searches at the LHC. In the latter, new decay channels open up, leading to longer decay chains and more complex experimental signatures. These two benchmark scenarios can be regarded as limiting cases, with "intermediate scenarios", where the heavier scalar masses lie in-between those values, leading to exclusion limits which lie within the two extreme cases. For these scenarios we have analyzed the present theoretical and experimental constraints.

We reinterpret a set of experimental searches for supersymmetric particles at the LHC by ATLAS within the framework of the RSIII with help of the package CheckMATE. In order to do this we implemented the model in high energy physics tools and generated the NP events which are then processed further by CheckMATE. The process with the most sensitive signature turns out to be pair-production of charged NP fermions, decaying each to the DM candidate and an electron or a muon. The resulting experimental signature, opposite sign dileptons plus MET, is also obtained in two supersymmetric processes: slepton pair-production decaying to the LSP and a lepton, or chargino-neutralino pair-production decaying subsequently via intermediate sleptons, where one of the charged leptons is lost in the detector. The fermion triplets decay via Yukawa couplings to a lepton and a scalar. Since these Yukawa couplings are intrinsically related to the neutrino mass matrix, a determination of the flavor structure of the final state would allow to directly study neutrino properties at colliders. It is therefore highly relevant to obtain exclusion limits as a function of the flavor structure of the final state. We have expressed those limits as a function of the branching ratio of the charged $\mathbf{Z}_2$-odd fermion to the DM candidate plus an electron or a muon. In the "best case scenario", with decoupled heavy scalars, the strongest limits on the $\mathbf{Z}_2$-odd fermion triplets are obtained in the e-philic case, for which we exclude masses below roughly 660 GeV. This limit is reduced to 640 GeV and 570 GeV, in, respectively, the mu-philic and e-mu symmetric cases. One should notice that our results are subject to uncertainties of the Monte Carlo simulations of the analysis which may be reduced with higher statistics. For light NP fermions, below roughly 150 GeV, the dilepton searches included in CheckMATE fail to exclude

our model. In order to obtain solid lower limits on the $\mathbf{Z}_2$-odd fermion masses we recast an analysis by ATLAS [54] for searches in the compressed mass spectra region. The experimental results included in CheckMATE are not sensitive to final state taus, which mostly generate hadron activity excluded in their cut-based analyses. We recast the results of [54] for tau searches, taking into account the larger cross-sections for fermion pair-production, to obtain a lower mass limit of around 400 GeV for fermion triplets in the tau-philic case. In the "worst case scenario" we have obtained limits both including only the primary decays to the DM candidate, and including all channels. The results in both cases are consistent with each other, with a slight gain in exclusion sensitivity in latter case, albeit at the price of a huge increase in computational effort. We have therefore restricted our analysis to the former case. The branching ratios are reduced by a factor of almost four, reducing the sensitivity to the level of slepton searches. In the e-philic and mu-philic cases we can exclude fermion triplet masses below roughly 380 and 360 GeV, respectively. As in the "best case scenario", the lower mass region is excluding by a recast of the compressed spectra analysis [54]. For the tau-philic case no limits can yet be set. The LHC exclusion limits obtained in flavor space on our scotogenic model, the RSIII, should be easily extended to all NP models with NLOP fermions in the adjoint representation of $SU(2)_L$ decaying to a scalar DM candidate and a lepton.

Appendix A.

CL_s method

The exclusion limits for N experimental channels were obtained combining them with the CL_s method defined in Ref. [135, 136]. The leading uncertainties coming from the background is convoluted with the individual channel likelihoods $\mathcal{L}(n_k; s_k + b_k)$ and $\mathcal{L}(n_k; b_k)$ for the signal plus background and background hypotheses, respectively, with a Gaussian distribution with standard deviation σ_{b_k},

$$\langle \mathcal{L}(n_k; s_k + b_k) \rangle = \frac{1}{\sqrt{2\pi}\sigma_{b_k}} \int_0^\infty db'_k \exp\left(-\frac{(b'_k - b_k)^2}{2\sigma_{b_k}^2} \right) \frac{e^{-(s_k+b'_k)}(s_k + b'_k)^{n_k}}{n_k!} , \quad \text{(A.1)}$$

with $\langle \mathcal{L}(n_k; b_k) \rangle$ defined analogously. Here n_k, s_k and b_k denote, respectively, the number of events, the expected signal events, and the corresponding background events in each channel.

The likelihood ratio test-statistics function is given by

$$Q = \prod_{i=1}^{N} \left(\frac{e^{-(s_i+b_i)}(s_i + b_i)^{n_i}/n_i!}{e^{-b_i} b_i^{n_i}/n_i!} \right) = e^{-s_{tot}} \prod_{i=1}^{N} \left(1 + \frac{s_i}{b_i} \right)^{n_i} , \quad \text{(A.2)}$$

with $s_{tot} = \sum_k^{N_n} s_k$. The observed likelihood ratio test statistics Q_{obs} is defined analogously setting $n_i = n_i^{obs}$, the observed number of events reported in the experimental analyses. The test statistics function Q should also be averaged by the Gaussian distribution. To simplify the numerical evaluation we average $\log Q$ as in Eq. (A.1)

$$\bar{Q} \equiv \exp(\langle \log Q \rangle) . \quad \text{(A.3)}$$

The confidence level for exclusion $\mathrm{C}L = 1 - CL_s$ is given by

$$CL_s = \frac{CL_{s+b}}{CL_b} \ , \tag{A.4}$$

with

$$CL_{s+b} = \sum_{\bar{Q}<\bar{Q}_{obs}} \prod_{k=1}^{N} \langle \mathcal{L}(n_k; s_k + b_k) \rangle \ , \tag{A.5}$$

$$CL_b = \sum_{\bar{Q}<\bar{Q}_{obs}} \prod_{k=1}^{N} \langle \mathcal{L}(n_k; b_k) \rangle \ . \tag{A.6}$$

Bibliography

[1] G. Palacio, Int. J. Mod. Phys. **A**31, 1650142 (2016), arXiv:1608.08676.

[2] F. von der Pahlen, G. Palacio, D. Restrepo, and O. Zapata, Phys. Rev. **D**94, 033005 (2016), arXiv:1605.01129.

[3] Super-Kamiokande, Y. Fukuda *et al.*, Phys. Rev. Lett. **8**1, 1562 (1998), arXiv:hep-ex/9807003.

[4] SNO, Q. R. Ahmad *et al.*, Phys. Rev. Lett. **8**9, 011301 (2002), arXiv:nucl-ex/0204008.

[5] SNO, Q. R. Ahmad *et al.*, Phys. Rev. Lett. **8**9, 011302 (2002), arXiv:nucl-ex/0204009.

[6] K2K, M. H. Ahn *et al.*, Phys. Rev. **D**74, 072003 (2006), arXiv:hep-ex/0606032.

[7] F. Zwicky, Helv. Phys. Acta **6**, 110 (1933).

[8] S. Weinberg, Phys. Rev. Lett. **4**3, 1566 (1979).

[9] P. Minkowski, Phys. Lett. **B**67, 421 (1977).

[10] R. N. Mohapatra and G. Senjanovic, Phys. Rev. Lett. **4**4, 912 (1980).

[11] M. Magg and C. Wetterich, Phys. Lett. **B**94, 61 (1980).

[12] J. Schechter and J. W. F. Valle, Phys. Rev. **D**22, 2227 (1980).

[13] T. P. Cheng and L.-F. Li, Phys. Rev. **D**22, 2860 (1980).

[14] G. B. Gelmini and M. Roncadelli, Phys. Lett. **B**99, 411 (1981).

[15] R. Foot, H. Lew, X. G. He, and G. C. Joshi, Z. Phys. **C**44, 441 (1989).

[16] A. Melfo, M. Nemevsek, F. Nesti, G. Senjanovic, and Y. Zhang, Phys. Rev. **D**85, 055018 (2012), arXiv:1108.4416.

[17] Z.-L. Han, R. Ding, and Y. Liao, Phys. Rev. **D**91, 093006 (2015), arXiv:1502.05242.

[18] Z.-L. Han, R. Ding, and Y. Liao, Phys. Rev. **D**92, 033014 (2015), arXiv:1506.08996.

[19] R. Franceschini, T. Hambye, and A. Strumia, Phys. Rev. **D**78, 033002 (2008), arXiv:0805.1613.

[20] J. A. Aguilar-Saavedra, P. M. Boavida, and F. R. Joaquim, Phys. Rev. **D**88, 113008 (2013), arXiv:1308.3226.

[21] ATLAS, G. Aad *et al.*, Phys. Rev. **D**92, 032001 (2015), arXiv:1506.01839.

[22] R. Foot and O. F. Hernandez, Phys. Rev. **D**41, 2283 (1990), [Erratum: Phys. Rev.D42,948(1990)].

[23] T. Gherghetta, N. Nagata, and M. Shifman, Phys. Rev. **D**93, 115010 (2016), arXiv:1604.01127.

[24] R. Foot, Phys. Rev. **D**83, 114013 (2011), arXiv:1103.1940.

[25] F. Pisano and V. Pleitez, Phys. Rev. **D**46, 410 (1992), arXiv:hep-ph/9206242.

[26] R. Foot, H. N. Long, and T. A. Tran, Phys. Rev. **D**50, R34 (1994), arXiv:hep-ph/9402243.

[27] Riazuddin and Fayyazuddin, Eur. Phys. J. **C**56, 389 (2008), arXiv:0803.4267.

[28] D. A. Gutierrez, W. A. Ponce, and L. A. Sanchez, Eur. Phys. J. **C**46, 497 (2006), arXiv:hep-ph/0411077.

[29] W. A. Ponce, Y. Giraldo, and L. A. Sanchez, p. 341 (2002), arXiv:hep-ph/0201133, [AIP Conf. Proc.623,341(2002)].

[30] A. Palcu, Mod. Phys. Lett. **A**21, 2591 (2006), arXiv:hep-ph/0605155.

[31] D. Cogollo, H. Diniz, and C. A. de S. Pires, Phys. Lett. **B**677, 338 (2009), arXiv:0903.0370.

[32] M. E. Catano, R. Martinez, and F. Ochoa, Phys. Rev. **D**86, 073015 (2012), arXiv:1206.1966.

[33] D. Cogollo, H. Diniz, and C. A. de S. Pires, Phys. Lett. **B**687, 400 (2010), arXiv:1002.1944.

[34] J. M. Cabarcas and J. A. Rodriguez, Mod. Phys. Lett. **A**29, 1450032 (2014),

arXiv:1303.5332.

[35] D. Cogollo, (2014), arXiv:1411.2810.

[36] D. Cogollo, Int. J. Mod. Phys. **A**30, 1550038 (2015), arXiv:1409.8115.

[37] K. Y. Lee and S.-h. Nam, J. Phys. **G**42, 125003 (2015), arXiv:1412.1541.

[38] P. Langacker, Phys. Rept. **7**2, 185 (1981).

[39] F. del Aguila, M. Masip, and J. L. Padilla, Phys. Lett. **B**627, 131 (2005), arXiv:hep-ph/0506063.

[40] J. Lee, (2005), arXiv:hep-ph/0504136.

[41] A. Abada, G. Bhattacharyya, and M. Losada, Phys. Rev. **D**73, 033006 (2006), arXiv:hep-ph/0511275.

[42] F. Bonnet, M. Hirsch, T. Ota, and W. Winter, JHEP **1**207, 153 (2012), arXiv:1204.5862.

[43] D. Aristizabal Sierra, A. Degee, L. Dorame, and M. Hirsch, JHEP **0**3, 040 (2015), arXiv:1411.7038.

[44] D. Restrepo, O. Zapata, and C. E. Yaguna, JHEP **1**311, 011 (2013), arXiv:1308.3655.

[45] E. Ma and D. Suematsu, Mod.Phys.Lett. **A**24, 583 (2009), arXiv:0809.0942.

[46] W. Chao, Int. J. Mod. Phys. **A**30, 1550007 (2015), arXiv:1202.6394.

[47] H. P. Nilles, Phys. Rept. **1**10, 1 (1984).

[48] H. E. Haber and G. L. Kane, Phys. Rept. **1**17, 75 (1985).

[49] R. Barbieri, Riv. Nuovo Cim. **1**1N4, 1 (1988).

[50] CERN Report No. ATLAS-CONF-2013-049, 2013 (unpublished).

[51] ATLAS Collaboration, G. Aad *et al.*, JHEP **1**404, 169 (2014), arXiv:1402.7029.

[52] ATLAS Collaboration, G. Aad *et al.*, JHEP **1**405, 071 (2014), arXiv:1403.5294.

[53] CMS, V. Khachatryan *et al.*, Eur. Phys. J. **C**74, 3036 (2014), arXiv:1405.7570.

[54] ATLAS, G. Aad *et al.*, Phys. Rev. **D**93, 052002 (2016), arXiv:1509.07152.

[55] D. V. Forero, M. Tortola, and J. W. F. Valle, Phys. Rev. **D**90, 093006 (2014), arXiv:1405.7540.

[56] M. Drees, H. Dreiner, D. Schmeier, J. Tattersall, and J. S. Kim, Comput. Phys. Commun. **1**87, 227 (2014), arXiv:1312.2591.

[57] M. Cacciari and G. P. Salam, Phys.Lett. **B**641, 57 (2006), arXiv:hep-ph/0512210.

[58] M. Cacciari, G. P. Salam, and G. Soyez, JHEP **0**804, 063 (2008), arXiv:0802.1189.

[59] CMS, V. Khachatryan *et al.*, JHEP **0**4, 018 (2017), arXiv:1610.04870.

[60] LEP SUSY Working Group (ALEPH, DELPHI, L3, OPAL) Report No. Notes LEPSUSYWG/01-03.1, 04-01.1, http://lepsusy.web.cern.ch/lepsusy/Welcome.html.

[61] A. Ashtekar, Nuovo Cim. **B**122, 135 (2007), arXiv:gr-qc/0702030.

[62] J. H. Schwarz and N. Seiberg, Rev. Mod. Phys. **7**1, S112 (1999), arXiv:hep-th/9803179.

[63] A. Pilaftsis, J. Phys. Conf. Ser. **1**71, 012017 (2009), arXiv:0904.1182.

[64] J. Iliopoulos, Introduction to the Standard Model of the Electro-Weak Interactions, in *Proceedings, 2012 European School of High-Energy Physics (ESHEP 2012): La Pommeraye, Anjou, France, June 06-19, 2012*, pp. 1–30, 2014, arXiv:1305.6779.

[65] Particle Data Group, K. A. Olive *et al.*, Chin. Phys. **C**38, 090001 (2014).

[66] A. Zee, Phys. Lett. **B**93, 389 (1980), [Erratum: Phys. Lett.B95,461(1980)].

[67] X.-G. He, Eur. Phys. J. **C**34, 371 (2004), arXiv:hep-ph/0307172.

[68] K. S. Babu, Phys. Lett. **B**203, 132 (1988).

[69] K. L. McDonald and B. H. J. McKellar, (2003), arXiv:hep-ph/0309270.

[70] E. Ma, Phys. Rev. **D**73, 077301 (2006), arXiv:hep-ph/0601225.

[71] A. Palcu, Int. J. Mod. Phys. **A**24, 4923 (2009), arXiv:0902.3756.

[72] W. A. Ponce and L. A. Sanchez, Mod. Phys. Lett. **A**22, 435 (2007), arXiv:hep-ph/0607175.

[73] H. Georgi, Front. Phys. **5**4, 1 (1982).

[74] A. Palcu, Mod. Phys. Lett. **A**24, 2589 (2009), arXiv:0908.1636.

[75] H. N. Long, L. T. Hue, and D. V. Loi, Phys. Rev. **D**94, 015007 (2016), arXiv:1605.07835.

[76] A. Palcu, Int. J. Theor. Phys. **5**6, 403 (2017), arXiv:1510.06717.

[77] A. Palcu, Phys. Rev. **D**85, 113010 (2012), arXiv:1111.6262.

[78] F. Pisano and V. Pleitez, Phys. Rev. **D**51, 3865 (1995), arXiv:hep-ph/9401272.

[79] F. J. Escrihuela, D. V. Forero, O. G. Miranda, M. Tortola, and J. W. F. Valle, Constraining right-handed neutrinos, in *Proceedings, 37th International Conference on High Energy Physics (ICHEP 2014): Valencia, Spain, July 2-9, 2014*, 2016, arXiv:1505.01097.

[80] MiniBooNE, A. A. Aguilar-Arevalo *et al.*, Phys. Rev. Lett. **1**10, 161801 (2013), arXiv:1207.4809.

[81] LENA, M. Wurm *et al.*, Astropart. Phys. **3**5, 685 (2012), arXiv:1104.5620.

[82] Z. Maki, M. Nakagawa, and S. Sakata, Prog. Theor. Phys. **2**8, 870 (1962).

[83] SINDRUM, U. Bellgardt *et al.*, Nucl. Phys. **B**299, 1 (1988).

[84] A. Merle and M. Platscher, Phys. Rev. **D**92, 095002 (2015), arXiv:1502.03098.

[85] A. Merle, M. Platscher, N. Rojas, J. W. F. Valle, and A. Vicente, (2016), arXiv:1603.05685.

[86] M. Hirsch *et al.*, JHEP **1**310, 149 (2013), arXiv:1307.8134.

[87] ATLAS, CMS, G. Aad *et al.*, Phys.Rev.Lett. **1**14, 191803 (2015), arXiv:1503.07589.

[88] M. Cirelli, N. Fornengo, and A. Strumia, Nucl.Phys. **B**753, 178 (2006), arXiv:hep-ph/0512090.

[89] Particle Data Group, J. Beringer *et al.*, Phys.Rev. **D**86, 010001 (2012).

[90] J. Casas and A. Ibarra, Nucl.Phys. **B**618, 171 (2001), arXiv:hep-ph/0103065.

[91] A. Anandakrishnan and C. S. Hill, Phys. Lett. **B**735, 412 (2014), arXiv:1403.4294.

[92] N. G. Deshpande and E. Ma, Phys. Rev. **D**18, 2574 (1978).

[93] A. Arhrib, Y.-L. S. Tsai, Q. Yuan, and T.-C. Yuan, JCAP **1**406, 030 (2014),

arXiv:1310.0358.

[94] G. C. Branco *et al.*, Phys. Rept. **5**16, 1 (2012), arXiv:1106.0034.

[95] S. Kanemura, T. Kubota, and E. Takasugi, Phys. Lett. **B**313, 155 (1993), arXiv:hep-ph/9303263.

[96] A. Arhrib, R. Benbrik, and N. Gaur, Phys. Rev. **D**85, 095021 (2012), arXiv:1201.2644.

[97] R. Barbieri, L. J. Hall, and V. S. Rychkov, Phys. Rev. **D**74, 015007 (2006), arXiv:hep-ph/0603188.

[98] M. Baak *et al.*, Eur.Phys.J. **C**72, 2003 (2012), arXiv:1107.0975.

[99] H. Okada, T. Toma, and K. Yagyu, Phys. Rev. **D**90, 095005 (2014), arXiv:1408.0961.

[100] R. Barbieri, A. Pomarol, R. Rattazzi, and A. Strumia, Nucl.Phys. **B**703, 127 (2004), arXiv:hep-ph/0405040.

[101] G. Cynolter and E. Lendvai, Eur.Phys.J. **C**58, 463 (2008), arXiv:0804.4080.

[102] G. Marandella, C. Schappacher, and A. Strumia, Nucl. Phys. **B**715, 173 (2005), arXiv:hep-ph/0502095.

[103] Gfitter Group, M. Baak *et al.*, Eur.Phys.J. **C**74, 3046 (2014), arXiv:1407.3792.

[104] ALEPH, A. Heister *et al.*, Phys. Lett. **B**583, 247 (2004).

[105] DELPHI, J. Abdallah *et al.*, Eur. Phys. J. **C**31, 421 (2003), arXiv:hep-ex/0311019.

[106] L3, M. Acciarri *et al.*, Phys. Lett. **B**472, 420 (2000), arXiv:hep-ex/9910007.

[107] OPAL, G. Abbiendi *et al.*, Eur. Phys. J. **C**35, 1 (2004), arXiv:hep-ex/0401026.

[108] A. Pierce and J. Thaler, JHEP **0**8, 026 (2007), arXiv:hep-ph/0703056.

[109] E. Lundstrom, M. Gustafsson, and J. Edsjo, Phys. Rev. **D**79, 035013 (2009), arXiv:0810.3924.

[110] CERN Report No. ATLAS-CONF-2015-044, 2015 (unpublished).

[111] T. Abe, R. Kitano, and R. Sato, Phys. Rev. **D**91, 095004 (2015), arXiv:1411.1335.

[112] P. Posch, Phys.Lett. **B**696, 447 (2011), arXiv:1001.1759.

[113] ATLAS, G. Aad *et al.*, Phys. Rev. **D**90, 112015 (2014), arXiv:1408.7084.

[114] CMS, V. Khachatryan *et al.*, Eur.Phys.J. **C**74, 3076 (2014), arXiv:1407.0558.

[115] A. Vicente and C. E. Yaguna, JHEP **0**2, 144 (2015), arXiv:1412.2545.

[116] MEG Collaboration, J. Adam *et al.*, Phys.Rev.Lett. **1**10, 201801 (2013), arXiv:1303.0754.

[117] Belle Collaboration, K. Abe *et al.*, Phys.Rev.Lett. **9**2, 171802 (2004), arXiv:hep-ex/0310029.

[118] Planck, P. A. R. Ade *et al.*, (2015), arXiv:1502.01589.

[119] LUX, D. S. Akerib *et al.*, Phys. Rev. Lett. **1**16, 161301 (2016), arXiv:1512.03506.

[120] Fermi-LAT, M. Ackermann *et al.*, (2015), arXiv:1503.02641.

[121] L. Lopez Honorez, E. Nezri, J. F. Oliver, and M. H. G. Tytgat, JCAP **0**702, 028 (2007), arXiv:hep-ph/0612275.

[122] E. M. Dolle and S. Su, Phys. Rev. **D**80, 055012 (2009), arXiv:0906.1609.

[123] L. Lopez Honorez and C. E. Yaguna, JHEP **0**9, 046 (2010), arXiv:1003.3125.

[124] L. Lopez Honorez and C. E. Yaguna, JCAP **1**101, 002 (2011), arXiv:1011.1411.

[125] D. Sokolowska, (2011), arXiv:1107.1991.

[126] M. Gustafsson, S. Rydbeck, L. Lopez-Honorez, and E. Lundstrom, Phys. Rev. **D**86, 075019 (2012), arXiv:1206.6316.

[127] G. Belanger, F. Boudjema, A. Pukhov, and A. Semenov, Comput.Phys.Commun. **1**85, 960 (2014), arXiv:1305.0237.

[128] B. Swiezewska and M. Krawczyk, Phys. Rev. **D**88, 035019 (2013), arXiv:1212.4100.

[129] A. Ibarra, E. Molinaro, and S. T. Petcov, JHEP **0**9, 108 (2010), arXiv:1007.2378.

[130] D. Aristizabal Sierra and C. E. Yaguna, JHEP **0**8, 013 (2011), arXiv:1106.3587.

[131] H. Baer *et al.*, (2013), arXiv:1306.6352.

[132] CMS Collaboration, CERN Report No. CMS-PAS-EXO-14-001, 2015 (unpublished).

[133] CMS Collaboration, CERN Report No. CMS-PAS-EXO-16-002, 2016 (unpublished).

[134] DELPHES 3, J. de Favereau *et al.*, JHEP **1**402, 057 (2014), arXiv:1307.6346.

[135] A. L. Read, Modified frequentist analysis of search results (The CL(s) method), in *Workshop on confidence limits, CERN, Geneva, Switzerland, 17-18 Jan 2000: Proceedings*, 2000.

[136] A. L. Read, J.Phys. **G**28, 2693 (2002).

[137] T. Junk, Nucl.Instrum.Meth. **A**434, 435 (1999), arXiv:hep-ex/9902006.

[138] A. Alloul, N. D. Christensen, C. Degrande, C. Duhr, and B. Fuks, Comput.Phys.Commun. **1**85, 2250 (2014), arXiv:1310.1921.

[139] J. Alwall *et al.*, (2014), arXiv:1405.0301.

[140] R. D. Ball *et al.*, Nucl. Phys. **B**867, 244 (2013), arXiv:1207.1303.

[141] T. Sjostrand, S. Mrenna, and P. Z. Skands, JHEP **0**605, 026 (2006), arXiv:hep-ph/0603175.

[142] W. Beenakker, R. Hopker, and M. Spira, (1996), arXiv:hep-ph/9611232.

[143] M. Cacciari, G. P. Salam, and G. Soyez, Eur.Phys.J. **C**72, 1896 (2012), arXiv:1111.6097.

List of Figures

2.1. realizations of the seesaw mechanism: Type I (left), Type II (in the middle) and Type III (right). The exchanged massive particle corresponds to a fermion singlet $N_R \sim (\mathbf{1}, \mathbf{1}, 0)$, a scalar triplet $\Delta \sim (\mathbf{1}, \mathbf{3}, -2)$ and a fermion triplet $\Sigma \sim (\mathbf{1}, \mathbf{3}, 0)$, respectively. 16

2.2. One-loop diagram in the Zee model. 20

2.3. Two-loop neutrino mass generation in the Babu model. 21

2.4. One-loop neutrino mass generation in the Ma model. 22

3.1. Topologies of the Weinberg-like effective operator. On the left hand side the intermediate particle could be an $SU(4)$ fermion singlet $N_R \sim (1, 0)$, and a fermion 15-plet $\Sigma \sim (15, 0)$. On the right hand side the intermediate particles could be an $SU(4)$ scalar decuplet $\Delta \sim (10, X_\Delta)$ and a scalar 15-plet $\Omega \sim (15, X_\Omega)$. 27

3.2. BR$(\mu^- \to e^+ e^- e^-)$ as a function of y_{ee}. The vertical dashed line represent the point where couplings of order $\sim 4\pi$ are expected, and the horizontal dashed line is the upper limit for BR$(\mu^- \to e^+ e^- e^-)$ process. 35

4.1. One-loop neutrino mass generation in the RSIII via the exchange of a $\mathbf{Z}_2$-odd neutral scalar $\phi^0 = H^0, A^0$ and a $\mathbf{Z}_2$-odd fermion Σ_k^0. The neutrino interaction eigenstates are denote by $\hat{\nu_\alpha}$ and $\hat{\nu_\beta}$. 41

4.2. Normal (NH) and inverse (IH) hierarchy solutions in flavor space (visualized as described in[91]). For every set of normalized yukawa couplings squared $|\hat{Y}_\alpha|^2, \alpha = e, \mu, \tau$, the lightest neutrino mass m_{ν_k} of the obtained solutions is averaged logarithmically. 41

4.3. Feynman diagrams contributing to $\mu^- \to e^-\gamma$. Here $\phi^0 = H^0, A^0$. Not shown are the self-energy corrections leading to electron-muon mixing. . . 42

4.4. EWPO constraints in the $(m_{H^+} - m_{H^0})$,$(m_{A^0} - m_{H^0})$ plane. The regions allowed at 68% (green), 95% (yellow) and 99% (red) CL have been obtained from the new physics contributions to the oblique parameters S, T, U. The dashed line delimits from below the region which allows for the correct scalar DM relic density in the RSIII. All shown points correspond to scenarios which satisfy the constraints of Sec. 4.2 for $m_{H^0} < 80$ GeV. The gray area corresponds to $m_{H^0} > m_{A^0}$, the dotted lines are contours of constant $m_{A^0} - m_{H^0}$. 47

4.5. Constraints of the scalar sector of the RSIII in the $\Omega_{\rm DM}h^2, m_{H^0}$ plane. Green points satisfy all constraints of Sec. 4.2. Dark green (light green) points represent scenarios with $m_{A^0} - m_{H^0} < 8$ GeV ($m_{H^\pm} - m_{H^0} <$ 12 GeV), in which A^0–H^0 ($H^\pm$–H^0) co-annihilation is the dominant annihilation channel before freeze-out. The upper bound on the invisible Higgs decay width from the LHC (black curve) gives a lower bound on m_{H^0} except for the dark green points (H^0–A^0 co-annihilation scenarios). The remaining scenarios are excluded by Planck relic density measurement (light blue), LUX direct detection searches (yellow), Fermi-LAT indirect detection searches (red), LHC Higgs decay to photons (purple). The bound for the invisible Higgs decay for a naive projection at the LHC Run-II (ILC expected sensitivity) is shown as a dashed (dotted) black curve. The horizontal lines represent the 2σ band on the measured relic density. A vertical dashed gray line shows the threshold of Higgs decay to DM pairs. 49

4.6. The left panel (a) shows the main production channel for pair $\Sigma_1^-\Sigma_1^+$ at the LHC. The right panel (b) shows the main decay channels of $\Sigma_1^\pm$ to DM. Here q denotes quarks of the first generation and $\ell_\alpha = e, \mu, \tau$. . . . 52

4.7. Contours of constant $m_{\Sigma_1^+}$ for the present LHC exclusion sensitivity of the RSIII in the $\mathcal{B}_e, \mathcal{B}_\mu$ plane (a) and $\mathcal{A}_{e\mu}, (\mathcal{B}_e + \mathcal{B}_\mu)$ plane (b), for $m_{H^0} =$ 70 GeV and $m_{H^\pm} \approx m_{A^0} > m_{\Sigma_1^\pm}$. The flavor symmetric scenario with $\mathcal{B}_e = \mathcal{B}_\mu = \mathcal{B}_\tau$ is shown with a star. The shaded triangle in (a) is not physical. Both figures show the same results. In (b) the area above each contour is excluded for the corresponding NP fermion mass. 59

4.8. Present LHC exclusion sensitivity in the $m_{\Sigma_1^+}, (\mathcal{B}_e + \mathcal{B}_\mu)$ plane for $m_{H^0} = 70$ GeV and $m_{H^\pm} \approx m_{A^0} > m_{\Sigma_1^\pm}$, in the mu-phobic (red), e-phobic (blue) and e-mu-symmetric (green) scenarios. The flavor symmetric scenario with $\mathcal{B}_e = \mathcal{B}_\mu = \mathcal{B}_\tau$ is shown with a star. The region above each curve is excluded. 60

4.9. NLO production cross-section for charged $\mathbf{Z}_2$-odd fermion pairs at the LHC with 8 TeV center of mass energy (blue line) as a function of the fermion mass. The corresponding 95% CL exclusion limits for the tau-philic case, when they decay exclusively to a tau and the DM scalar, are shown for $m_{H^0} = 60$ GeV (red line, black dots) and 80 GeV (yellow line, white dots). The limits have been obtained from those derived in [54] for stau pair-production. Also shown is the LEP lower bound on $m_{\Sigma_1^\pm}$. 61

4.10. Exclusion confidence level CL as a function of the NP fermion mass in the "worst case scenario" of Eq. (4.27). The dots correspond to the e-philic case $\hat{Y}_e = 1$ (red), mu-philic case $\hat{Y}_\mu = 1$ (blue). The dashed lines simply connect the dots. Masses for which $1 - \text{CL} < 0.05$ are excluded. 62

List of Tables

2.1. The particle content of the SM. The generation index is represented by α and each up-type quark u^α and down-type one d^α, carries also color charge. 10

3.1. Particle content for models A and B, the $\alpha = \{1, 2, 3\}$ are the lepton generation indices, i run over the first two generations of quarks. The numbers in parentheses refer to the $(SU(3)_C, SU(4)_L, U(1)_X)$ quantum numbers respectively. 24

3.2. Particle content for models E and F, the $\alpha = \{1, 2, 3\}$ are the lepton generation indices, i run over the first two generations of quarks. The numbers in parentheses refer to the $(SU(3)_C, SU(4)_L, U(1)_X)$ quantum numbers respectively. 25

3.3. Scenarios for the operator defined in Eq. (3.6): In the left part, the $(4(\overline{4}), X_{L(\Phi)})$ notation represents the way as the fields (either $L_{L\alpha}$ or Φ_i) transforms under $SU(4)_L \otimes U(1)_X$. The effective operator is allowed if it is gauge invariant. 26

4.1. Gauge, $\mathbf{Z}_2$ and spin quantum numbers of the particle content of the RSIII entering $\mathcal{L}_{\rm NP}$, Eq. (4.2). Here α and k denote, respectively, the lepton flavor and NP fermion index. 38